DEVELOPMENTAL BIOLOGY

NAT10-mediated mRNA N^4-acetylation is essential for the translational regulation during oocyte meiotic maturation in mice

Lu Chen[1,2]†, Wen-Jing Wang[1]†, Shao-Yuan Liu[1]†, Rui-Bao Su[3]†, Yu-Ke Wu[1]†, Xuan Wu[1], Song-Ying Zhang[4], Jie Qiao[2], Qian-Qian Sha[5]*, Heng-Yu Fan[1,4,6]*

The precise translational regulation of maternal messenger RNAs (mRNAs) drives mammalian oocyte maturation. However, the function and mechanism of posttranscriptional chemical modifications, especially the newly identified N^4-acetylcytidine (ac^4C) modification catalyzed by *N*-acetyltransferase 10 (NAT10), are unknown. In this study, we developed a low-input ac^4C sequencing technology, ac^4C LACE-seq, and mapped 8241 ac^4C peaks at the whole-transcriptome level using 50 mouse oocytes at the germinal vesicle stage. Oocyte-specific *Nat10* knockout wiped out ac^4C signals in oocytes and caused severe defects in meiotic maturation and female infertility. Mechanically, *Nat10* deletion led to a failure of ac^4C deposition on mRNAs encoding key maternal factors, which regulate transcriptome stability and maternal-to-zygotic transition. *Nat10*-deleted oocytes showed decreased mRNA translation efficiency due to the direct inhibition of ac^4C sites on specific transcripts during meiotic maturation. In summary, we developed a low-input, high-sensitivity mRNA ac^4C profiling approach and highlighted the important physiological function of ac^4C in the precise regulation of oocyte meiotic maturation by enhancing translation efficiency.

INTRODUCTION

Mammalian oocyte maturation is driven by the strictly regulated polyadenylation and translational activation of maternal mRNA stored in the cytoplasm. Many mRNAs in germinal vesicle (GV) stage–arrested oocytes are stored within ribonucleoproteins that protect them from degradation (*1*). Selective polyadenylation and decapping are the central control mechanisms that lead to translational regulation, storage, and degradation (*2*, *3*). Mouse oocytes are an ideal model for studying the regulation of posttranscriptional cytoplasmic mRNA polyadenylation and translation because fully grown mammalian oocytes are transcriptionally quiescent, and the translation product of mRNA stored in the cytoplasm drives meiosis during early development (*4*). Little is known about how mRNA posttranscriptional modifications precisely regulate the translation process during oocyte meiotic maturation, and their specific physiological functions remain largely unknown.

With the innovation and development of high-throughput sequencing technology, "epitranscriptome" research has gradually emerged in recent years. It has become a hot topic in life sciences in the postgenomic era. The "epitranscriptome" consists of the chemical modifications that occur on the ribonucleotides of RNA after transcription (*5*). More than 170 chemical modifications have been found in the RNA of prokaryotes, archaea, and eukaryotes (*6*–*8*). To date, 11 chemical modifications have been detected in the cytosine nucleoside of RNA, including three types—5-methylcytidine (m^5C), 5-hydroxymethylcytidine (hm^5C), and N^4-acetylcytidine (ac^4C)—which are conserved in all living species (*6*). In recent years, an increasing number of studies have found that posttranscriptional modifications of mRNA are involved in various precise regulatory processes, such as RNA transport and output, splicing and processing, polyadenylation, stability, and degradation, to maintain mRNA turnover in organisms (*5*).

N^4-Acetylcytidine (ac^4C) was first found in yeast tRNA (*9*), and further studies found it in yeast $tRNA^{Leu}$ (*10*), *Escherichia coli* $tRNA^{Met}$ (*11*), and bacterial $tRNA^{Met}$ (*12*) and revealed that ac^4C modification of $tRNA^{Met}$ is critical for coding accuracy in protein synthesis (*13*). Subsequently, researchers detected ac^4C in eukaryotic 18S ribosomal RNA (rRNA) (*14*). In 2018, a study detected ac^4C modifications in the mRNA of human HeLa cells for the first time and proved that the ac^4C modification of mRNA was also catalyzed by *N*-acetyltransferase 10 (NAT10) (*15*). Further research has shown that ac^4C modification enhances mRNA stability and promotes translation efficiency (*15*). However, another study concluded that the ac^4C modification does not occur in human or yeast mRNA. Supporting evidence is that the research group has developed the transcriptome sequencing technology ac^4C-seq at a single-nucleotide resolution level (*16*). Recently, we reported dynamic changes in the overall ac^4C modification abundance in the total RNA of different tissues and during spermatogenesis. Male germ cell–specific *Nat10* knockout disrupts the normal transcriptome of spermatogenic cells and leads to sterility in male mice, indicating that NAT10-mediated ac^4C modification has crucial physiological functions (*17*). However, the distribution of ac^4C modifications in the mRNA during oocyte maturation and the molecular mechanisms regulating this process remain unclear.

To date, researchers have developed various techniques to qualitatively or quantitatively detect ac^4C modifications in organisms, including high-performance liquid chromatography (*18*), reversed-phase high-performance liquid chromatography (*19*), liquid chromatography–tandem mass spectrometry (*20*), and capillary electrophoresis (*21*). Although these methods can detect ac^4C modifications to a certain extent, they cannot be used to conduct quantitative studies on the

[1]MOE Key Laboratory for Biosystems Homeostasis and Protection and Innovation Center for Cell Signaling Network, Life Sciences Institute, Zhejiang University, Hangzhou 310058, China. [2]State Key Laboratory of Female Fertility Promotion, Center for Reproductive Medicine, Department of Obstetrics and Gynecology, Peking University Third Hospital, Beijing 100191, China. [3]Fertility Preservation Laboratory, Reproductive Medicine Center, Guangdong Second Provincial General Hospital, Guangzhou 510317, China. [4]Zhejiang Key Laboratory of Precise Protection and Promotion of Fertility, Department of Obstetrics and Gynecology, Sir Run Run Shaw Hospital, School of Medicine, Zhejiang University, Hangzhou 310016, China. [5]College of Life Science, Guangzhou Medical University, Guangzhou 511436, China. [6]Center for Biomedical Research, Shaoxing Institute, Zhejiang University, Shaoxing 312000, China.
*Corresponding author. Email: hyfan@zju.edu.cn (H.-Y.F.); shaqianqian@zju.edu.cn (Q.-Q.S.)
†These authors contributed equally to this work.

distribution of ac^4C. "Epitranscriptome" research in the postgenomic era relies on the innovation and development of various high-throughput sequencing technologies. In recent years, with the development of ac^4C-specific antibodies (*22*), researchers have developed ac^4C-RNA immunoprecipitation and sequencing (acRIP-seq) on the basis of ac^4C antibodies (*15*). Although the above detection methods have promoted ac^4C-related research to a certain extent, they cannot be used to study the precise distribution pattern and dynamic change process of ac^4C modification in the transcriptome, markedly limiting detailed studies of the physiological functions of ac^4C modification. Over the past 3 years, researchers have found that sodium borohydride and its derivatives can reduce the ac^4C modification of RNA under acidic conditions. Mismatches occur at sites where reduction reactions occur during reverse transcription. Combined with Sanger sequencing, the specific locations and numbers of mismatches can be detected (*16*, *23*–*25*). However, this method is similar to acRIP-seq in that the library construction process relies on a higher input of samples, which limits the application of these two methods to microvolume samples, such as germ cells and early embryos. Therefore, an urgent need is to develop ac^4C sequencing technology with high sensitivity, single-nucleotide resolution, and low-input amounts.

Recently, researchers have developed a linear amplification of complementary DNA ends and sequencing (LACE-seq) method to identify RNA binding protein (RBP) targets in low-input samples, including oocytes. In this approach, the RBP binding site is directly obtained by linearly amplifying the termination signal of the reverse transcriptase at the RBP binding site. This technology accurately identified RBP binding sites at single-base resolution and the single cell level (*26*). This study optimized and improved the critical steps of the previously reported LACE-seq method and established a low-input, high-sensitivity ac^4C LACE-seq technology suitable for oocyte and embryo ac^4C profiling. We mapped ac^4C peaks at the whole-transcriptome level in mouse oocytes at the GV stage. We constructed an oocyte-specific *Nat10* knockout mouse model to study the physiological function of ac^4C modification mediated by NAT10 during oocyte maturation. These studies revealed that *Nat10* deletion failed to establish ac^4C modification of essential genes functional in meiotic maturation and further disrupted oocyte maturation–associated mRNA translation activity.

RESULTS

NAT10 is expressed in oocytes and associated with the dynamic changes in the abundance of ac^4C

To investigate the potential function of NAT10 in mediating RNA ac^4C modification in mouse oocytes during growth and meiotic maturation, we detected the expression of *Nat10* mRNA and protein. Reverse transcription quantitative polymerase chain reaction (RT-qPCR) results showed that the expression level of *Nat10* transcripts was high at the GV stage and then continued to decrease until the lowest expression level was observed at the two-cell stage (Fig. 1A). In addition, we analyzed the published data on the expression of RNA and protein of NAT10 during meiosis of wild-type (WT) mouse oocytes (*27*, *28*). The results showed that both RNA and protein were gradually decreased with the maturation of the oocyte (fig. S1, A and B). Western blotting results also indicated that the expression of NAT10 is high in GV oocytes and gradually decreased during the maternal-to-zygotic transition (MZT) process (Fig. 1B). Immunofluorescence staining revealed that NAT10 was mainly localized around the nucleolus and nucleoplasm of GV oocytes. After meiotic resumption and GV breakdown (GVBD), NAT10 distributed in the ooplasm at metaphase I (MI) and metaphase II (MII). NAT10 gradually accumulated in the pronuclei after fertilization (Fig. 1C). We further overexpressed pDEST-mCherry-NAT10 via a plasmid and in vitro–transcribed mRNA in HeLa cells and GV oocytes separately. The results showed that NAT10 localizes to the nucleolus and nucleoplasm in somatic cells and GV oocytes (fig. S1, C and D). Recent studies have detected RNA chemical modifications through immunofluorescence staining, such as m^6A (*29*–*31*), m^5C (*32*), and ac^4C (*33*). Therefore, to detect the presence of RNA ac^4C modifications in mouse oocytes and preimplantation embryos, we performed immunofluorescence staining using an ac^4C antibody. The results showed that the ac^4C signal was present in the nucleus and cytoplasm of oocytes and preimplantation embryos, with the strongest signal in the nucleolus of fully grown GV oocytes (Fig. 1D). Ribosomal RNA is the most abundant RNA in cells, and previous studies have confirmed that ac^4C modifications occur in rRNA (*34*–*36*). This explains the notable accumulation of the ac^4C signal in the nucleolus. After the resumption of meiosis in oocytes, ac^4C signals are diffused in the ooplasm. After fertilization, ac^4C signals relocated to nucleolus-like structures (Fig. 1D), consistent with the expression pattern of the NAT10 protein (Fig. 1C). These results indicate that NAT10 is dynamic in mouse oocytes. Its expression pattern was consistent with the changes in ac^4C localization and levels, suggesting that NAT10 plays a crucial role in regulating RNA ac^4C modification during oogenesis.

To confirm whether the deletion of *Nat10* in oocytes caused a reduction in the overall RNA ac^4C modification level, we collected GV stage oocytes from WT and *Nat10*$^{fl/fl}$*;Gdf9-Cre* mice and performed NAT10 and ac^4C immunofluorescence staining. The results showed that the NAT10 signal was undetectable in oocytes from *Nat10*$^{fl/fl}$*;Gdf9-Cre* mice (Fig. 1E) and that the ac^4C signals in *Nat10*-deleted oocytes were significantly reduced (Fig. 1, F and G), proving that the RNA ac^4C modifications detected in WT oocytes were mediated by NAT10. This result also confirmed that the NAT10 and ac^4C signals detected using immunofluorescence were specific.

LACE-seq results show ac^4C modifications on transcripts in mouse oocytes

Inspired by the LACE-seq technology, we optimized the method and developed the ac^4C LACE-seq in this study. The difference with the LACE-seq technology is that we first incubated ac^4C antibodies with oocyte lysates, followed by ultraviolet (UV) cross-linking to cross-link ac^4C antibodies with RNA-containing ac^4C in cells to produce a steric hindrance effect. The subsequent steps are carried out according to LACE-seq (*26*). Briefly, antibody-incubated magnetic beads were further used to specifically enrich "ac^4C antibody-RNA complexes" from cell lysates. To digest RNA into single ac^4C-containing short fragments, the "ac^4C antibody-RNA complexes" on the magnetic beads were further treated with micrococcal nuclease. The 3′ end of the RNA fragment was then dephosphorylated and ligated with an adapter containing four random nucleotides and an adenylated 5′ end. Biotinylated primers containing a T7 promoter were then used for reverse transcription on beads, cDNA was enriched using streptavidin beads, and 14 to 18 cycles of PCR were performed to achieve linear amplification of trace amounts of truncated cDNA, thereby obtaining a specific modification of ac^4C at the whole-transcriptome level. The technical

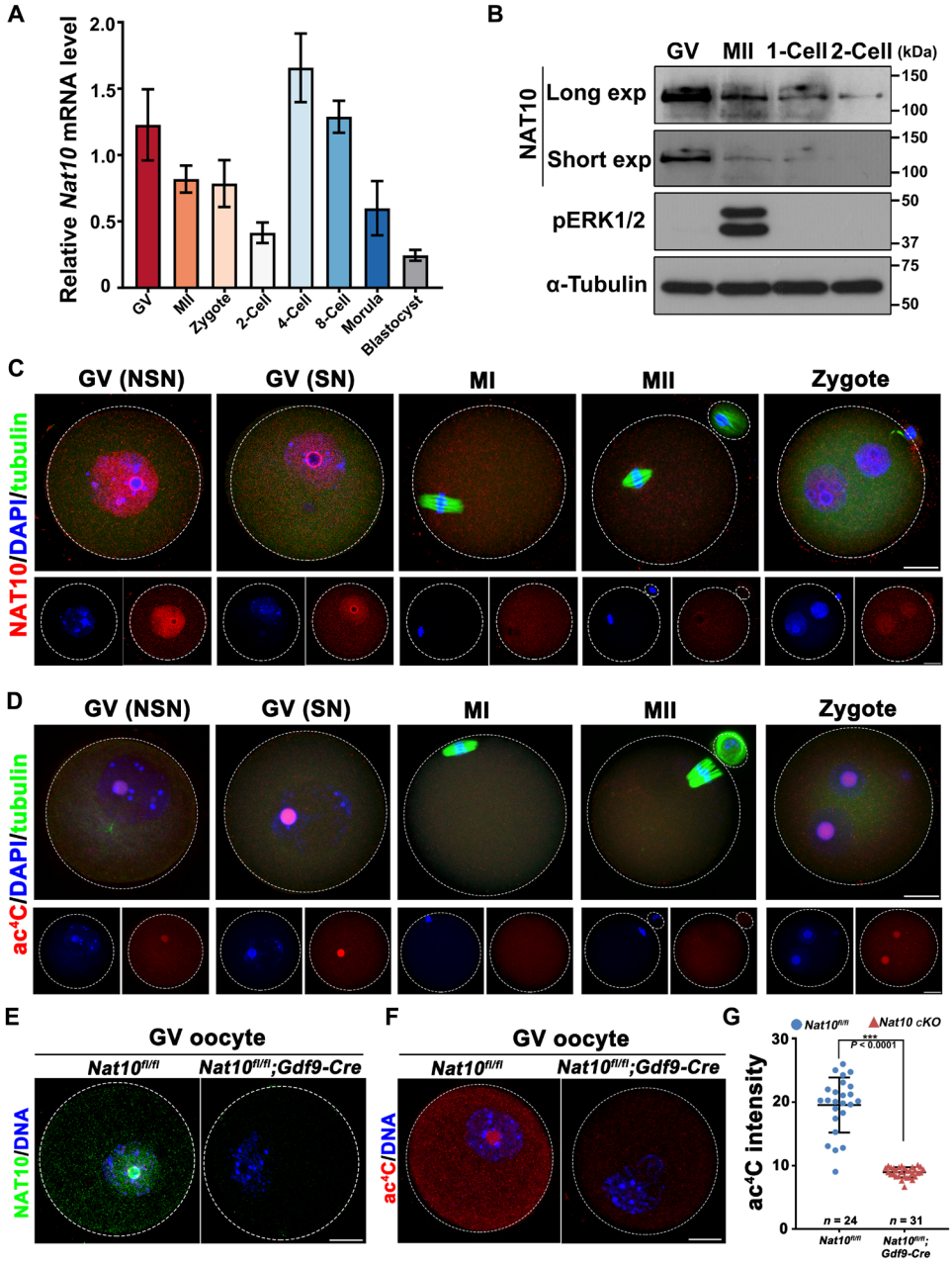

Fig. 1. Expression and localization of NAT10 in oocytes and preimplantation embryos. (**A**) RT-qPCR results showing the level changes of *Nat10* transcripts during mouse oocyte maturation and preimplantation embryonic development. (**B**) The expression of NAT10 during the MZT stages was detected using Western blotting (100 oocytes or embryos per lane). (**C** and **D**) Immunofluorescence results showing the expression and localization of NAT10 and ac^{4}C during mouse oocyte meiotic maturation and fertilization. (**E** and **F**) Immunofluorescence results showing the expression and localization of NAT10 and ac^{4}C in WT and *Nat10*-deleted oocytes. (**G**) Quantitative statistics of the ac^{4}C fluorescence signal in (E). Scale bars, 20 μm for all panels in (C) to (F).

route is shown in Fig. 2A and Materials and Methods. To further confirm the credibility of the ac^{4}C peaks captured by LACE-seq, we performed LACE-seq on transcripts interacting with NAT10, the only known ac^{4}C writer protein (Fig. 2A).

On the basis of this optimized ac^{4}C LACE-seq method, we collected 50 WT GV oocytes for ac^{4}C and NAT10 LACE-seq library construction and two replicates were set for each group of samples. The obtained LACE-seq data were then filtered for rRNA reads, and non-rRNA reads were retained for subsequent analysis. The LACE-seq data obtained in each group had a higher mapping rate (table S1). The results showed that the quality of the data received at this starting amount was highly reliable, and the correlation between the two biological replicates in the WT GV oocyte NAT10 LACE-seq and ac^{4}C LACE-seq results was 80% (fig. S2A and table S2). The overlap ratio between the two biological repeats was high in ac^{4}C and NAT10 LACE-seq. Thus, we considered the overlapping peaks of biological repeats as credible ac^{4}C peaks (8241) and NAT10 binding peaks (4243) for subsequent analysis (Fig. 2, B and C, and tables S3 to S8).

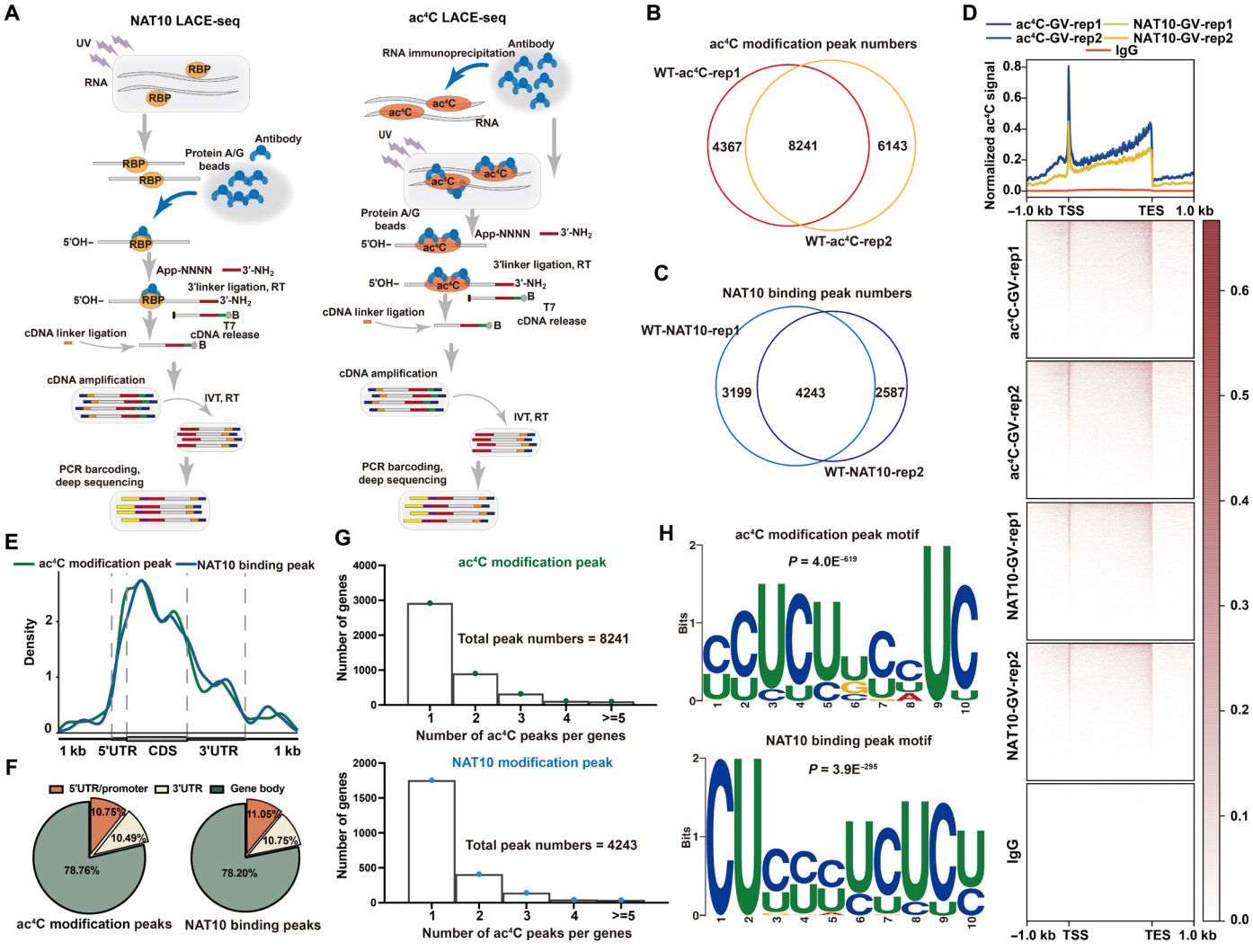

Fig. 2. Identification of ac^{4}C on maternal transcripts in mouse oocytes using a LACE-seq–based approach. (**A**) Technical diagram of NAT10 LACE-seq (left) and ac^{4}C LACE-seq (right). (**B**) Overlap of ac^{4}C peaks from two biological replicates in WT GV oocytes. (**C**) Overlap of NAT10 binding peaks from two independent experiments in WT GV oocytes. (**D**) Distributions and heatmap of ac^{4}C and NAT10 binding peaks on the genome. IgG served as a negative control. (**E**) Distribution patterns of ac^{4}C-modified and NAT10-RNA–interacting sites in the transcriptome. (**F**) Distribution ratio of ac^{4}C and NAT10 binding peaks in each transcript region. (**G**) Histogram showing the average number of NAT10 and ac^{4}C binding peaks per gene in WT GV oocyte. (**H**) Motif enrichment analyses of ac^{4}C and NAT10 binding peaks.

In comparison, almost no ac^{4}C or NAT10 signals were detected in the immunoglobulin G (IgG) group, indicating that the peaks captured by the ac^{4}C and NAT10 antibodies were specific (Fig. 2D). Further analyses revealed that the ac^{4}C peaks and NAT10 binding peaks had consistent distribution patterns in the genome, with higher signals enriched near the transcription start signal (TSS) and transcription ending signal (TES) (Fig. 2D). The peaks detected by both ac^{4}C and NAT10 antibodies mainly distributed in the coding-sequenced and 5′ untranslated regions (5′UTR) (Fig. 2, E and F). Further analysis of the 8241 ac^{4}C and 4243 NAT10 binding peaks showed that most detected transcripts carry one to two peaks (Fig. 2G). The ac^{4}C and NAT10 binding peak motifs were CU enriched (Fig. 2H). The distribution pattern and motif of ac^{4}C peaks identified in this study are consistent with those of previous reports (*15*, *37*). These results further verified that the ac^{4}C signal obtained by ac^{4}C LACE-seq has high sensitivity and reliability.

ac^{4}C LACE-seq results have good reproducibility with previously published data and in cross-analyses

To verify the reliability and reproducibility of the ac^{4}C LACE-seq method, we performed joint analyses of ac^{4}C LACE-seq data and acRIP-seq results in GV oocytes (*38*). The authors performed acRIP-seq on 2000 GV stage oocytes in this study and identified 6188 transcripts carrying ac^{4}C peaks (*38*). In our study, only 50 GV stage oocytes were used, and 8241 ac^{4}C peaks (7461 transcripts) were collectively captured in both sets of replicates (Fig. 2B). To compare our ac^{4}C LACE-seq results with published acRIP-seq results, we recalled peaks according to the same standards and parameters, analyzed the data from the two databases simultaneously, and performed ac^{4}C signal normalization with fragments per kilobase of transcript per million mapped fragments (FPKM). The results show that the ac^{4}C signals detected by ac^{4}C LACE-seq were more robust than those detected by acRIP-seq (Fig. 3A). Chromosomes 5 and 10 were selected

to display the overall ac^{4}C peaks using Integrative Genomics Viewer, and the signals captured by ac^{4}C LACE-seq and NAT10 LACE-seq were stronger than those of acRIP-seq (Fig. 3B and fig. S2B). Signals of ac^{4}C peaks were detected in transcripts of key maternal genes, including nuclear polyadenylate-binding protein 1 (*Pabpn1*), B cell translocation gene 4 (*Btg4*), and poly(A) binding protein interacting protein 2 (*Paip2*). The results showed that ac^{4}C LACE-seq had stronger sensitivity than acRIP-seq in GV stage oocytes (Fig. 3, C and D, and fig. S2C). To compare the reproducibility of ac^{4}C-containing transcripts captured by the two different methods, comparative analyses of the ac^{4}C-containing mRNAs obtained by the two other methods revealed 4891 shared mRNAs and 81% of the ac^{4}C-associated mRNAs identified by acRIP-seq were detected in our ac^{4}C LACE-seq (Fig. 3E), indicating that the ac^{4}C detection technology optimized in this study has high reproducibility and that the database generated by this technology is credible.

We further compared the results of ac^{4}C and NAT10 LACE-seq; 52.5% (2227 of 4243) of the targets captured by the NAT10 antibody were also captured by ac^{4}C LACE-seq (fig. S2D), and motif enrichment analysis of 2227 ac^{4}C peaks cotargeted by ac^{4}C LACE-seq and NAT10 LACE-seq showed significant "CU" enrichment (fig. S2E). Furthermore, the peaks captured by the ac^{4}C antibody had more notable signal enrichment in the peak center regions than those captured by the NAT10 antibody (Fig. 3F). This is consistent with our speculation because the ac^{4}C antibody directly recognizes the modification site. In contrast, the NAT10 antibody only targets NAT10-interacting transcript regions mediated by other RBPs; the peaks captured by NAT10 LACE-seq are the ac^{4}C peaks recognized by the

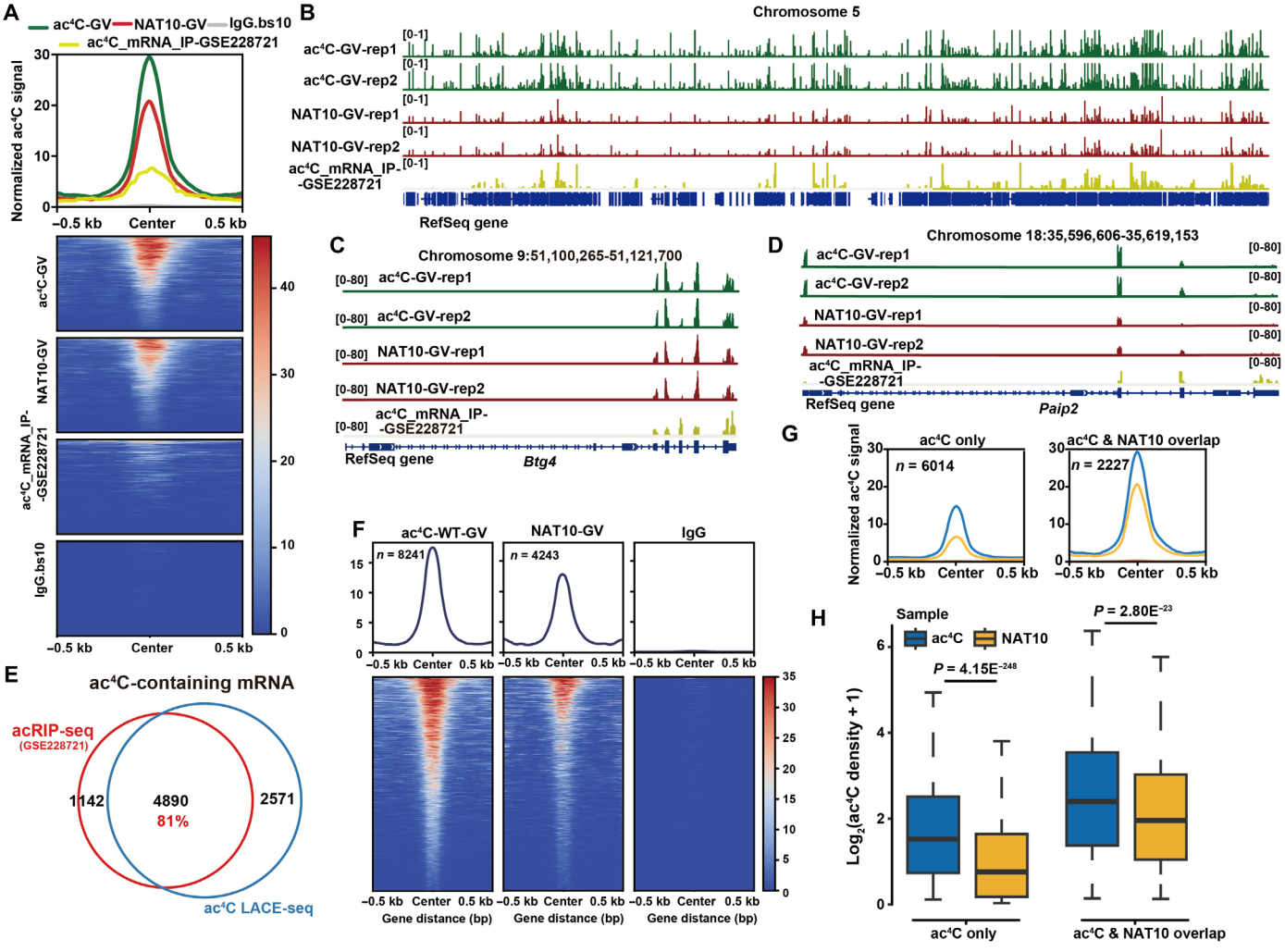

Fig. 3. Comparative analyses of oocyte ac^{4}C LACE-seq and oocyte acRIP-seq. (**A**) Meta profile and heatmap of signals from ac^{4}C LACE-seq, NAT10 LACE-seq, and acRIP-seq (GSE228721) around the identified peak center. IgG served as a control. (**B**) UCSC genome browser views of ac^{4}C LACE-seq, NAT10 LACE-seq, and acRIP-seq reads on chromosome 5. (**C** and **D**) UCSC genome browser views of distributions of peaks obtained by ac^{4}C LACE-seq, NAT10 LACE-seq, and acRIP-seq of *Btg4* (C) and *Paid2* (D). Both are key oocyte maturation genes. (**E**) Overlapping targeted peaks by ac^{4}C LACE-seq and acRIP-seq in GV stage oocytes. (**F**) The heatmap shows the peak signals captured by ac^{4}C LACE-seq and NAT10 LACE-seq in GV oocytes, and the IgG group is set as a negative control. (**G**) The ac^{4}C peak signal intensity normalization analysis was performed on the peaks captured only by ac^{4}C LACE-seq and the peak signals cotargeted by ac^{4}C and NAT10. (**H**) Boxplot showing that ac^{4}C and NAT10 targets have a higher ac^{4}C density than ac^{4}C-only targets. One-tailed unpaired Student's *t* test calculated the *P* value. The center line represents the median, the box borders represent the first and third quartiles, and the whiskers are the most extreme data points within 1.5 × the interquartile range.

"NAT10-adaptor" complex. Similar to the trend in Fig. 3F, the signal intensities of the peaks captured only by ac^{4}C LACE-seq were higher than those captured by NAT10 LACE-seq alone (Fig. 3G). Further quantitative analysis of the ac^{4}C signal intensity in these two groups (ac^{4}C-only and ac^{4}C and NAT10 overlap) showed that the overlapping group had higher signal intensity than the ac^{4}C-only group peak signal (Fig. 3H). Collectively, these results confirmed the reliability of the ac^{4}C LACE-seq method and indicated that ac^{4}C LACE-seq is a low-input, high-sensitivity, and high-reproducibility approach for profiling ac^{4}C modifications at the transcriptome level.

NAT10 is essential for female fertility and oocyte meiotic maturation

Nat10 knockout mice are embryonically lethal (*39*). To study the in vivo function of NAT10, we generated *Nat10*$^{fl/fl}$*;Gdf9-Cre* conditional knockout mice that specifically inactivate *Nat10* expression in oocytes at the primordial follicle stage. Similar to the immunofluorescence results shown in Fig. 1E, immunohistochemical staining of ovarian paraffin sections of *Nat10*$^{fl/fl}$*;Gdf9-Cre* mice showed that the NAT10 protein was not detected in oocytes at all follicle stages (Fig. 4A). Western blot results indicated that NAT10 was expressed in GV oocytes and down-regulated in MII oocytes after meiotic maturation but was undetectable in oocytes from *Nat10*$^{fl/fl}$*;Gdf9-Cre* mice (Fig. 4B). These results demonstrate that *Nat10* is efficiently and specifically inactivated in *Nat10*$^{fl/fl}$*;Gdf9-Cre* mice. For fertility tests, we crossed *Nat10*$^{fl/fl}$*;Gdf9-Cre* and *Nat10*$^{fl/fl}$ female mice with WT male mice for 6 months. *Nat10*$^{fl/fl}$*;Gdf9-Cre* female mice were completely sterile, suggesting that *Nat10* is essential for reproduction in female mice.

To determine the causes of female infertility, we evaluated the in vivo maturation of oocytes in WT and *Nat10*$^{fl/fl}$*;Gdf9-Cre* mice after superovulation treatment. In *Nat10*-deleted oocytes collected from the oviducts, the polar body 1 (PB1) emission rate was consistent with that in the control group (Fig. 4C). However, immunofluorescence staining of α-tubulin in the ovulated MII oocytes revealed that the proportion of spindle abnormalities significantly increased after *Nat10* deletion (Fig. 4, D and E). Targeting protein for XKLP2 (TPX2) and pericentrin are important proteins for spindle assembly. Immunofluorescence staining showed that the loss of *Nat10* resulted in disordered spindle assembly and abnormal localization of pericentrin (Fig. 4F), and the fluorescence intensity of TPX2 on the spindles was significantly reduced (Fig. 4G). We collected ovulated MII oocytes and performed chromosomal spreading and immunofluorescence staining. The results showed that *Nat10* deletion increased aneuploidy in MII oocytes (Fig. 4, H and I). We further evaluated oocyte meiotic maturation using in vitro culture experiments. The results showed that GVBD and PB1 emission rates were significantly reduced in *Nat10*-deleted oocytes compared with WT (Fig. 4J). Immunofluorescence staining revealed that the proportion of spindle abnormalities in MII stage oocytes of *Nat10*$^{fl/fl}$*;Gdf9-Cre* mice exceeded 90% under in vitro culture conditions (Fig. 4, K and L).

To evaluate the developmental potential of these oocytes, we performed superovulation on *Nat10*$^{fl/fl}$*;Gdf9-Cre* female mice, mated them with WT male mice, and collected fertilized eggs from the oviducts. The normal pronucleus formation rate was significantly reduced after *Nat10* deletion, and the proportion of abnormal pronuclei increased (Fig. 4M). These results further confirm the meiotic maturation defects and reduced fertilization potential of *Nat10*-deficient oocytes.

Loss of *Nat10* results in reduced global mRNA ac^{4}C modification

To study the ac^{4}C modification changes in transcripts caused by *Nat10* deletion at the whole-transcriptome level, we collected 50 GV stage oocytes from WT and *Nat10*$^{fl/fl}$*;Gdf9-Cre* mice for ac^{4}C LACE-seq and set up IgG LACE-seq as the control. The results showed that the ac^{4}C signal was enriched in the WT oocytes and was higher near the TSS and TES sites (Fig. 5A). When *Nat10* was deleted, the ac^{4}C signal in GV stage oocytes was significantly reduced to levels comparable to those in the negative control group (Fig. 5A). The ac^{4}C signals were enriched in WT GV oocytes within 0.5 kb upstream and downstream of the putative ac^{4}C modification center, with a total of 8241 modification sites. When deleting *Nat10*, the ac^{4}C signal within 0.5 kb upstream and downstream of the ac^{4}C modification site is globally reduced. Only 215 ac^{4}C modification sites with weak signals were detected (Fig. 5B). Gene Ontology analysis results indicated that most of the mRNAs carrying NAT10-dependent ac^{4}C modifications encoded proteins involved in mRNA processing, ribonucleoproteins biogenesis, RNA splicing, and translation (Fig. 5C and table S9). In addition, most ac^{4}C-containing genes are enriched in autophagy, tight junction, polycomb repressive complex, cell cycle, and oocyte meiosis pathways (fig. S3A and table S10), consistent with the phenotype in the present study. We selected five key maternal mRNAs that accumulated abundantly in oocytes to visualize the ac^{4}C peaks through Integrative Genomics Viewer (Fig. 5, D to F; and fig. S3, B and C). Among these, *Msy2*, *Pabpn1*, zygote arrest 1 (*Zar1*), and *Btg4* are involved in regulating mRNA translation and stability. Multiple ac^{4}C peaks were detected in these transcripts using both ac^{4}C and NAT10 LACE-seq in WT oocytes. However, after *Nat10* knockout, the ac^{4}C peaks of these transcripts almost completely disappeared (Fig. 5, D to F; and fig. S3, B and C). These results further suggest that the ac^{4}C peaks detected by ac^{4}C LACE-seq in the WT oocytes are accurate and specific because the oocytes from *Nat10*-deleted mice serve as a stringent negative control.

Transcript deregulation caused by *Nat10* deletion is not significantly related to ac^{4}C density

To investigate how reduced ac^{4}C modification caused by *Nat10* deletion leads to meiotic defects, we collected GV oocytes from WT and *Nat10*$^{fl/fl}$*;Gdf9-Cre* mice for transcriptome sequencing. RNA sequencing (RNA-seq) results showed high correlation among the three biological samples (fig. S4A). PCA (principal component analysis) was performed on these samples, and the results showed that the principal components between WT and *Nat10*-deleted oocytes were not significantly different (PCA2 = 2.41%) (fig. S4B), indicating that *Nat10* deletion did not have a significant impact on the overall transcriptome stability. The RNA-seq results were analyzed for differentially expressed genes (DEGs) [$\log_2$ fold change (FC) > 1 or $\log_2$FC < −1, $P < 0.05$] (tables S11 and S12). The volcano plot shows that the loss of *Nat10* resulted in the down-regulation and up-regulation of 930 and 1093 transcripts in GV oocytes (Fig. 6A). We further analyzed the relationship between mRNA ac^{4}C modifications and the oocyte transcriptome. To more rigorously define which genes may carry ac^{4}C modification, we adopted two different conditions and then took their intersection to consider the mRNA with ac^{4}C modification, as shown in Fig. 6B: on the left, the low-abundance background signals detected in ac^{4}C LACE-seq were eliminated through the screening of FPKM > 1, while on the right, the gene set with high

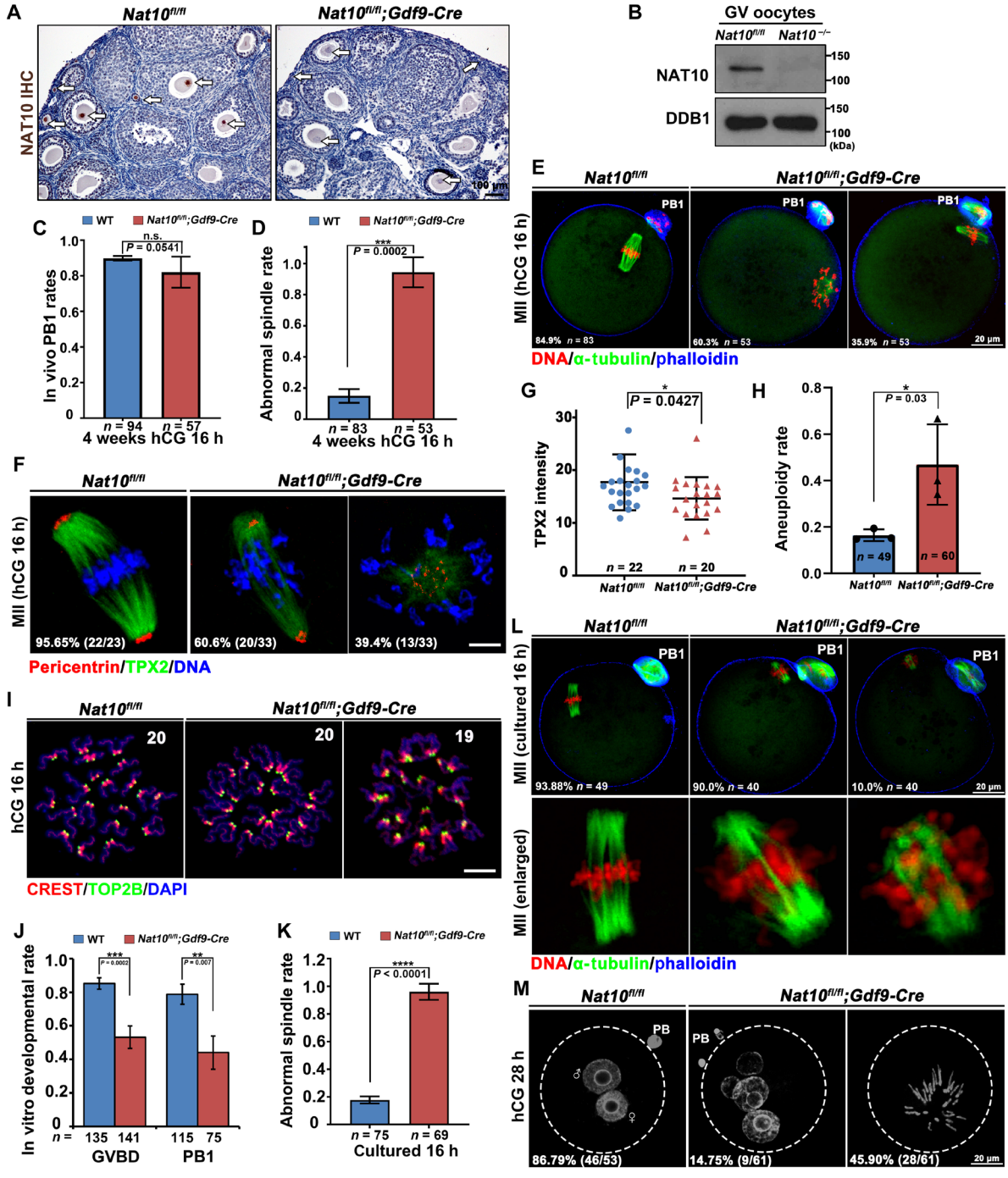

Fig. 4. *Nat10* deletion results in oocyte maturation defects. (**A**) Immunohistochemistry results indicate that the NAT10 protein was abolished in oocytes within ovarian follicles of *Nat10*-cKO mice. Scale bar, 100 μm. (**B**) Western blot results showing NAT10 protein levels in oocytes of WT and *Nat10*$^{fl/fl}$;*Gdf9-Cre* mice. The total proteins of 100 oocytes were loaded in each lane. A constitutively expressed protein DDB1 was blotted as a loading control. (**C**) Statistics on the proportion of the PB1 emissions in oocytes ovulated by WT and *Nat10*$^{fl/fl}$;*Gdf9-Cre* mice at 16 hours (h) after hCG injection. n.s., not significant. (**D**) Ratio of abnormal spindles in ovulated MII oocytes. (**E**) Immunofluorescence staining to detect spindle assembly and chromosome arrangement in MII oocytes of WT and *Nat10*$^{fl/fl}$;*Gdf9-Cre* mice. (**F**) Immunofluorescence was used to detect the expression and localization of TPX2 and pericentrin proteins in MII stage oocytes ovulated by WT and *Nat10*$^{fl/fl}$;*Gdf9-Cre* mice. Scale bar, 10 μm. (**G**) Quantifications of TPX2 immunofluorescence signal intensity in (F). (**H**) Statistics on the proportion of chromosomal aneuploidy in MII stage oocytes ovulated by WT and *Nat10*$^{fl/fl}$;*Gdf9-Cre* mice. (**I**) Chromosome spreading combined with immunofluorescence detection of chromosomal euploidy in MII oocytes ovulated by WT and *Nat10*$^{fl/fl}$;*Gdf9-Cre* mice. Scale bar, 10 μm. (**J**) Meiotic resumption (characterized by GVBD and PB1 emission rates) of WT and *Nat10*-deleted oocytes cultured in vitro. (**K**) Ratio of abnormal spindles in WT and *Nat10*-deleted oocytes cultured in vitro. (**L**) Immunofluorescence staining to detect spindle assembly and chromosome arrangement in WT and *Nat10*-deleted oocytes at 16 hours after in vitro culture. Scale bars, 20 μm. (**M**) Detection of pronucleus formation by DAPI immunofluorescence staining in fertilized eggs derived from WT and *Nat10*$^{fl/fl}$;*Gdf9-Cre* female mice. Scale bar, 20 μm.

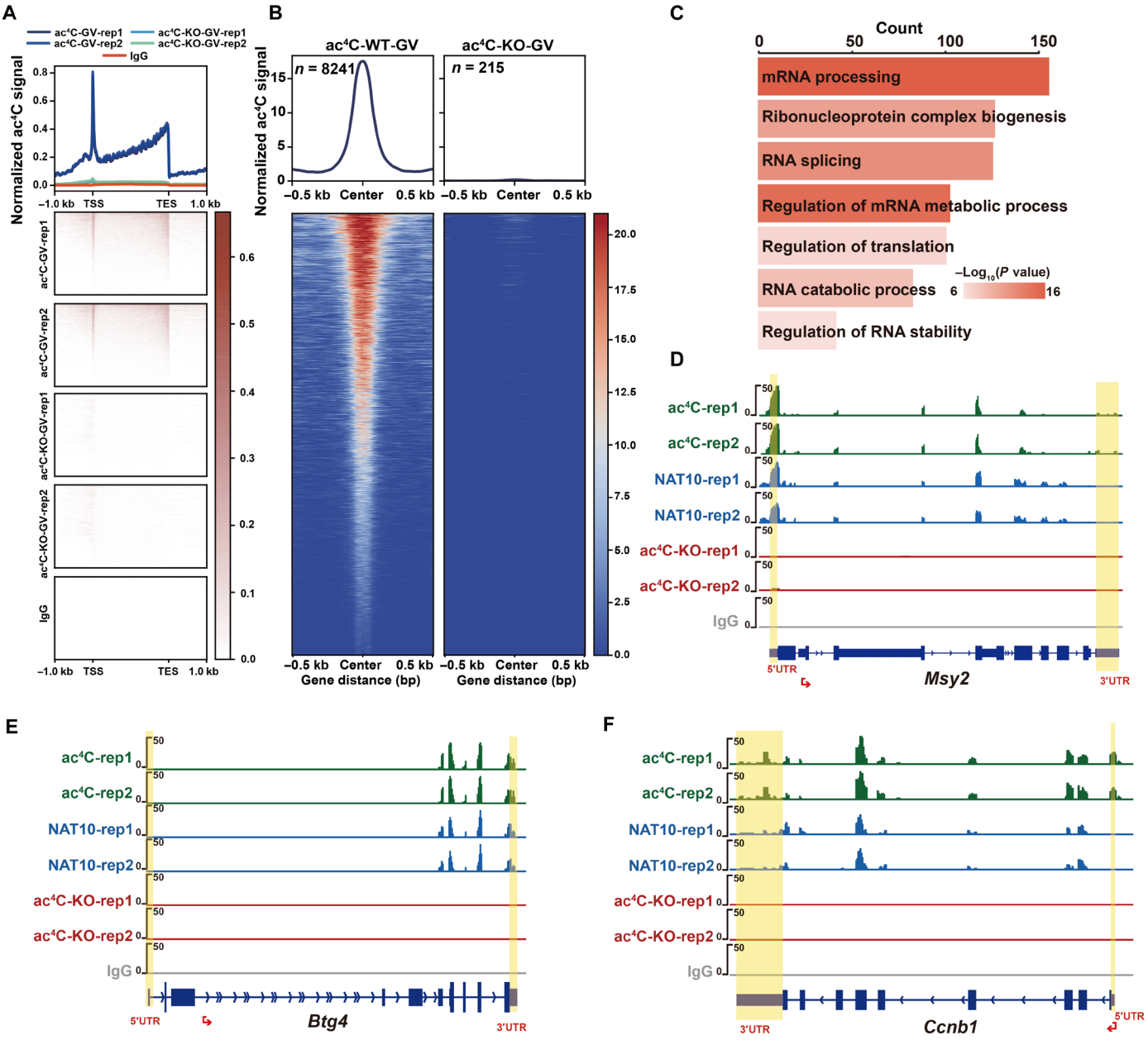

Fig. 5. Loss of *Nat10* results in reduced ac^{4}C modifications on mRNAs. (**A**) ac^{4}C LACE-seq detects ac^{4}C modification in GV stage oocytes from WT and *Nat10*$^{fl/fl}$;*Gdf9-Cre* mice. (**B**) Meta profile and heatmap of ac^{4}C signals around the identified peak center from WT and *Nat10*$^{fl/fl}$;*Gdf9-Cre* mice. (**C**) Gene Ontology enrichment analysis was performed on genes with ac^{4}C peaks significantly reduced after *Nat10* deletion. (**D** to **F**) UCSC genome browser views of abolished ac^{4}C peaks on the key maternal genes (*Msy2*, *Btg4*, and *Ccnb1*) at the GV stage of WT and *Nat10*$^{fl/fl}$;*Gdf9-Cre* mice.

ac^{4}C LACE-seq peaks was obtained through the more rigorous call peak function of MACS2 software (FC > 2 and $P < 0.001$), thereby defining the 2366 overlapping genes as strict ac^{4}C$^+$ genes (Fig. 6B). Next, we performed an overlap analysis of the DEGs caused by *Nat10* deletion and the ac^{4}C$^+$ genes. The results showed that only 59 differentially expressed transcripts were ac^{4}C$^+$ genes (Fig. 6C), indicating that NAT10-mediated ac^{4}C modification did not significantly affect the stability of ac^{4}C$^+$ transcripts in GV oocytes.

Further joint analysis of the ac^{4}C$^+$ transcripts with the maternal-decay, zygotic-decay, and zygotic genome activation–dependent transcripts defined in WT mice showed that 54 and 34% of ac^{4}C$^+$ transcripts were maternal-decay and zygotic-decay transcripts, respectively. Another 12% of transcripts were zygotic genome activation dependent (fig. S4C). To analyze the relationship between ac^{4}C modification and gene expression, we divided the ac^{4}C$^+$ transcripts into two clusters on the basis of the changes in expression during the MZT in WT mice (fig. S4, D and E). Among them, there were 1113 transcripts in cluster II, which were gradually degraded during meiotic maturation and then maintained at low levels (fig. S4E). This suggests that most ac^{4}C$^+$ transcripts are highly expressed in GV oocytes and may play an essential role in meiotic maturation.

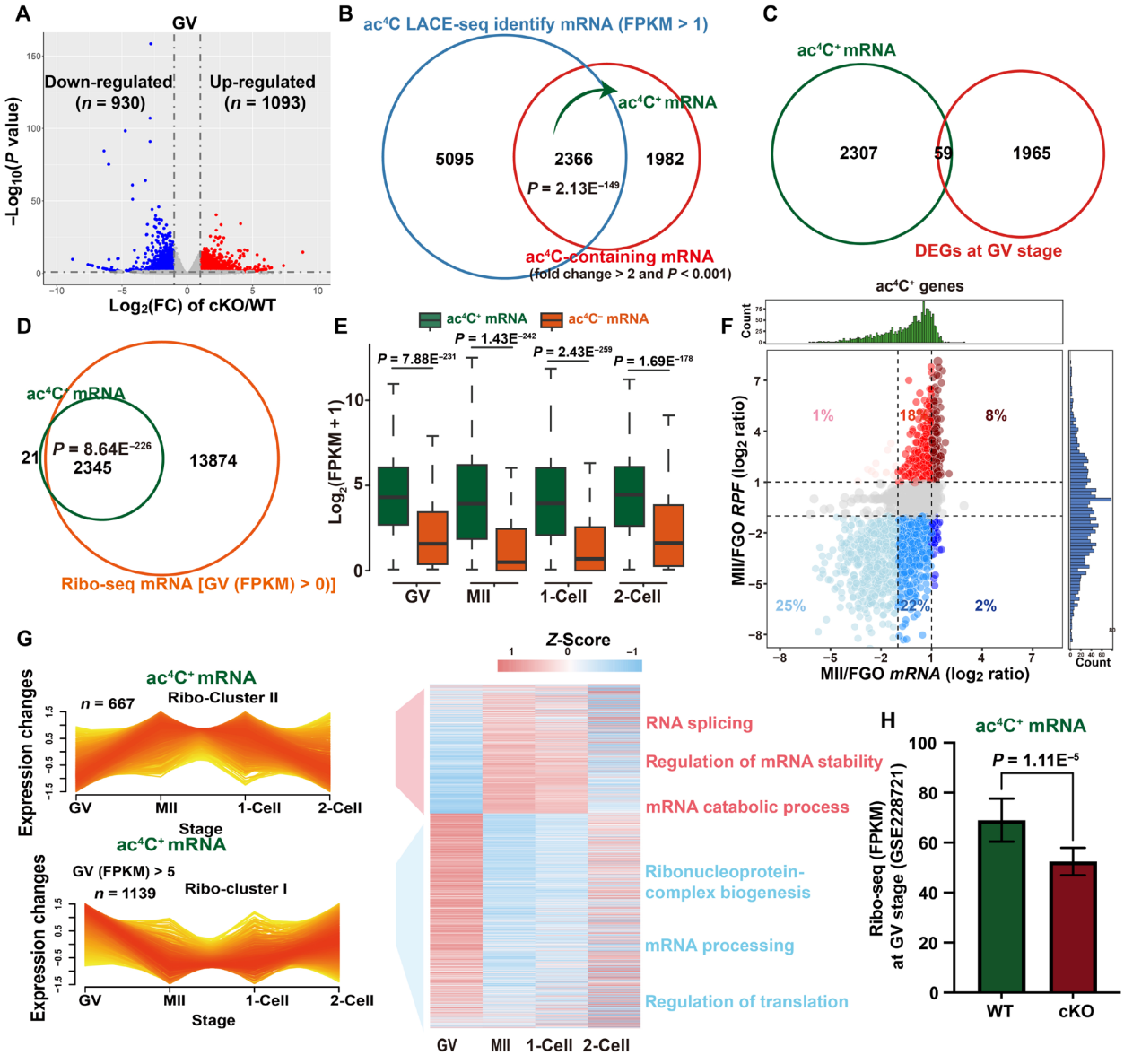

Fig. 6. ac^{4}C modification couples to translation during oocyte meiotic maturation. (**A**) Volcano plots show the number of significantly differentially expressed genes (DEGs) in GV oocytes of WT and *Nat10*-cKO mice. $P = 0.05$ and $\log_2 FC = \pm 1$ are reported in gray horizontal and vehicle dashed lines, respectively. *n*, gene number. (**B**) The expression level corresponding to the 7461 transcripts carrying ac^{4}C peaks is limited to FPKM > 1, and the gene set with high ac^{4}C peaks was obtained through MACS2 software (FC > 2 and $P < 0.001$). The overlapped 2366 genes are defined as strictly ac^{4}C$^+$ genes. (**C**) Overlap analysis was conducted between ac^{4}C$^+$ transcripts (B) and DEGs (A) in GV oocytes. (**D**) Venn diagram showing the overlap between strict ac^{4}C$^+$ transcripts and ribosome-bound transcripts in GV oocytes. (**E**) Boxplot showing the dynamic changes of Ribo-lite FPKM of ac^{4}C$^+$ and ac^{4}C$^-$ transcripts during GV to the two-cell stage. The *P* value was calculated using a one-tailed unpaired Student's *t* test. (**F**) Scatter plots showing the ac^{4}C$^+$ transcript dynamic changes (FC, *x* axis) and Ribo-lite dynamic change (FC, *y* axis) from GV to MII. Red and blue plots show that the translatome up-regulated or down-regulated more than twofold change in the MII stage compared with GV. (**G**) 2366 ac^{4}C$^+$ transcripts were jointly analyzed with Ribo-seq data during the MZT process. They were divided into two clusters on the basis of Ribo-seq expression changes. Heatmap showing dynamic changes during MZT. The enriched GO terms are also listed. Histogram showing the translatome of the ac^{4}C$^+$ transcripts in published Ribo-seq data (*27*, *38*) in WT and *Nat10*-null GV oocytes. The *P* value was calculated using a one-tailed unpaired Student's *t* test. Error bars, SEM. (**H**) Joint analysis of the ac^{4}C$^+$ genes in this study with the published Ribo-seq data in WT and *Nat10*-null GV oocytes (*38*).

RNA ac^{4}C modification couples to translation efficiency during oocyte meiotic maturation

Precise translation regulation is a core biological event that occurs during the meiotic maturation of oocytes. To investigate whether ac^{4}C modification is required for oocyte meiotic maturation by affecting translation activity, we compared 2366 ac^{4}C$^+$ transcripts with the translational omics database in GV oocytes identified using Ribo-lite (*27*). Almost all ac^{4}C$^+$ transcripts showed high translational activity (ribosome binding efficiency) in GV oocytes (Fig. 6D). Compared with ac^{4}C$^-$ transcripts, ac^{4}C$^+$ transcripts had higher translational activity at the GV, MII, one-cell, and two-cell stages (Fig. 6E). In addition, we further jointly analyzed the mRNA and ribosome-protected mRNA fragments of ac^{4}C$^+$ genes from the GV to MII stages, which revealed that the respective translation

efficiencies (49 and 27%) of the ac^{4}C$^+$ genes were significantly reduced (blue area below) and increased (red area above). Although 22% of the ac^{4}C$^+$-containing genes' mRNAs were stable from GV to MII, their translation efficiency was also significantly reduced (middle blue area). Our results show that most ac^{4}C$^+$ transcripts had higher translational activity in GV than in MII oocytes (Fig. 6F). We divided the ac^{4}C$^+$ transcripts into two clusters on the basis of changes in their translational activity during the MZT process; 1139 of them belong to cluster I, with higher translational activity in the GV stage, and these transcripts are enriched in the biological processes of the ribonucleoprotein complex, mRNA processing, and regulation of translation (Fig. 6G). In comparison, fewer transcripts belonged to cluster II (n = 667), with relatively low translational activity at the GV stage (Fig. 6G). These results indicate a positive correlation between mRNA ac^{4}C modification and translational activity during oocyte meiotic maturation. To determine the relationship between ac^{4}C modification and translation activity, we further analyzed ribosome sequencing (Ribo-seq) results in GV oocytes of WT and *Nat10*$^{fl/fl}$;*Gdf9-Cre* mice (*38*). The results showed that when *Nat10* was deleted, the translation efficiency (fragments per kilobase million of the Ribo-seq results) of the ac^{4}C$^+$ transcripts was significantly reduced (Fig. 6H). The abolishment of ac^{4}C modification caused by *Nat10* deletion significantly reduces the translation efficiency of ac^{4}C$^+$ transcripts, highlighting the coupling of ac^{4}C modification and the translation activity of ac^{4}C-contain mRNAs during oocyte maturation.

Nat10 deletion and reduced ac^{4}C modification impair the translation of key maternal mRNAs

To further verify the impact of *Nat10* deletion on translation activity during the oocyte meiotic maturation, we performed the Click-iT L-homopropargylglycine (HPG) protein synthesis assay on oocytes at multiple stages of meiotic maturation to evaluate the overall translation activity in oocytes. The results showed that translation was rapidly activated as meiosis resumed in WT oocytes. In contrast, translation activity at all detected stages was reduced in *Nat10*-deleted oocytes (Fig. 7, A and B). Transcripts encoding key maternal proteins, including MSY2, PABPN1, and ZAR1, underwent ac^{4}C modifications at the GV stage, mainly in their coding sequences (Fig. 5D and fig. S3, B and C). Both Western blotting and immunofluorescence results indicated that MSY2, PABPN1, and ZAR1 protein expression levels were compromised in *Nat10*-deleted GV oocytes (Fig. 7, C and D). As shown in Fig. 7A, meiotic resumption–coupled translational activation was compromised in *Nat10*-deleted oocytes; we selected key proteins that need to be translationally activated during oocyte meiotic maturation for verification. Western blotting results showed that the expression of BTG4 and cyclin B1 proteins was significantly reduced in *Nat10*-deficient MII oocytes (Fig. 7E), and the ac^{4}C peaks on their coding genes (*Btg4* and *Ccnb1*) also decreased substantially after *Nat10* deletion (Fig. 5, E and F). In contrast, the mRNA levels of these key maternal genes were not significantly affected by *Nat10* deletion (Fig. 7F). This strongly supports the notion that the reduction of ac^{4}C caused by *Nat10* deficiency mainly affects the translation efficiency of maternal mRNA rather than transcript stability.

To further verify the impact of *Nat10* deletion on meiotic maturation–triggered translational activation, we selected two key maternal genes, *Btg4* and *Ccnb1*, to construct translation reporter plasmids, transcribed the mRNA in vitro, microinjected it together with *mCherry* mRNA into GV oocytes from WT and *Nat10*$^{fl/fl}$;*Gdf9-Cre* mice, and measured translational activity using the ratio of green fluorescent protein (GFP) and mCherry fluorescence intensity. After the injection of Flag-GFP-*Btg4*-3′UTR into WT GV oocytes, GFP was rapidly translationally activated after meiosis resumed. Both fluorescence and Western blotting results showed that the mRNA translation efficiency of Flag-GFP-*Btg4*-3′UTR was significantly reduced after *Nat10* deletion (Fig. 8, A to C). Similarly, the translation activity of Flag-GFP-*Ccnb1*-3′UTR mRNA was significantly reduced in both GV and MII oocytes of *Nat10*$^{fl/fl}$;*Gdf9-Cre* mice (Fig. 8, D to F). These results indicate that *Nat10* deletion affects the translation efficiency of maternal mRNAs in mouse oocytes during meiotic maturation.

Subsequently, we investigated the direct effects of mRNA ac^{4}C modifications on translation. We used PACES software (*40*) to predict potential ac^{4}C modification sites on candidate genes and mutated these "C" sites in the coding sequences of *Msy2* and *Zar1* without affecting the amino acid sequences (Fig. 9A). We then transfected 293T cells (which did not endogenously express MSY2 and ZAR1) with plasmids expressing WT (full-length forms of HA-ZAR1 and HA-MSY2) and ac^{4}C site–mutated *Msy2* and *Zar1* (C mutant forms of HA-MSY2$^{M366–383}$, HA-ZAR1$^{M141–155}$, HA-ZAR1$^{D141–155}$, HA-ZAR1$^{D378–392}$, and HA-ZAR1$^{D628–642}$) (table S13). Western blotting results showed that the ac^{4}C site mutation reduced the expression of MSY2 and ZAR1 (Fig. 9, B to D). To further verify whether enhancing ac^{4}C modification can promote mRNA translation efficiency, we increased the stoichiometry of ac^{4}C in specific transcripts by incorporating different ratios of ac^{4}CTP during in vitro transcription (Fig. 9E). We then microinjected GV stage–arrested oocytes with in vitro–transcribed GFP-ZAR1 mRNAs with or without ac^{4}C incorporation (Fig. 9E). The results showed that transcripts containing ac^{4}C had higher translational levels than those without the ac^{4}C incorporation (Fig. 9, F to H). These results provide valid evidence that the ac^{4}C modification of mRNAs could enhance translation in oocytes.

DISCUSSION

In this field, the controversy remains about whether ac^{4}C modification occurs on eukaryotic mRNA (*41*, *42*). This controversial conclusion mainly arises from two independent research groups that developed different ac^{4}C sequencing technologies and obtained inconsistent conclusions in HeLa cells. Arango *et al.* used antibody-based methods (acRIP-seq) to map ac^{4}C and showed the presence of 4251 acetylated regions in HeLa cells (*15*). In contrast, Sas-Chen *et al.* developed a quantitative and single-nucleotide resolution approach (ac^{4}C-seq) for the transcriptome-wide quantitative mapping of ac^{4}C sites, and the profiling results suggested that ac^{4}C is absent or present at a very low stoichiometry in human cell lines and yeast mRNA (*16*). The discrepancy between these two studies is likely due to the differences in detection methodologies. RNA modification profiling methods based on antibodies have been applied to detect various RNA modifications, such as m^{6}A (*29*, *30*) and m^{5}C (*32*). The accuracy of the detection results of this method depends on antibody specificity. It is necessary to exclude false-positive results caused by antibody cross-reactivity carefully; therefore, the reproducibility and specificity of these chemically modified peaks obtained by sequencing must be fully verified. However, the limitation of the antibody-based method is that it is impossible to identify

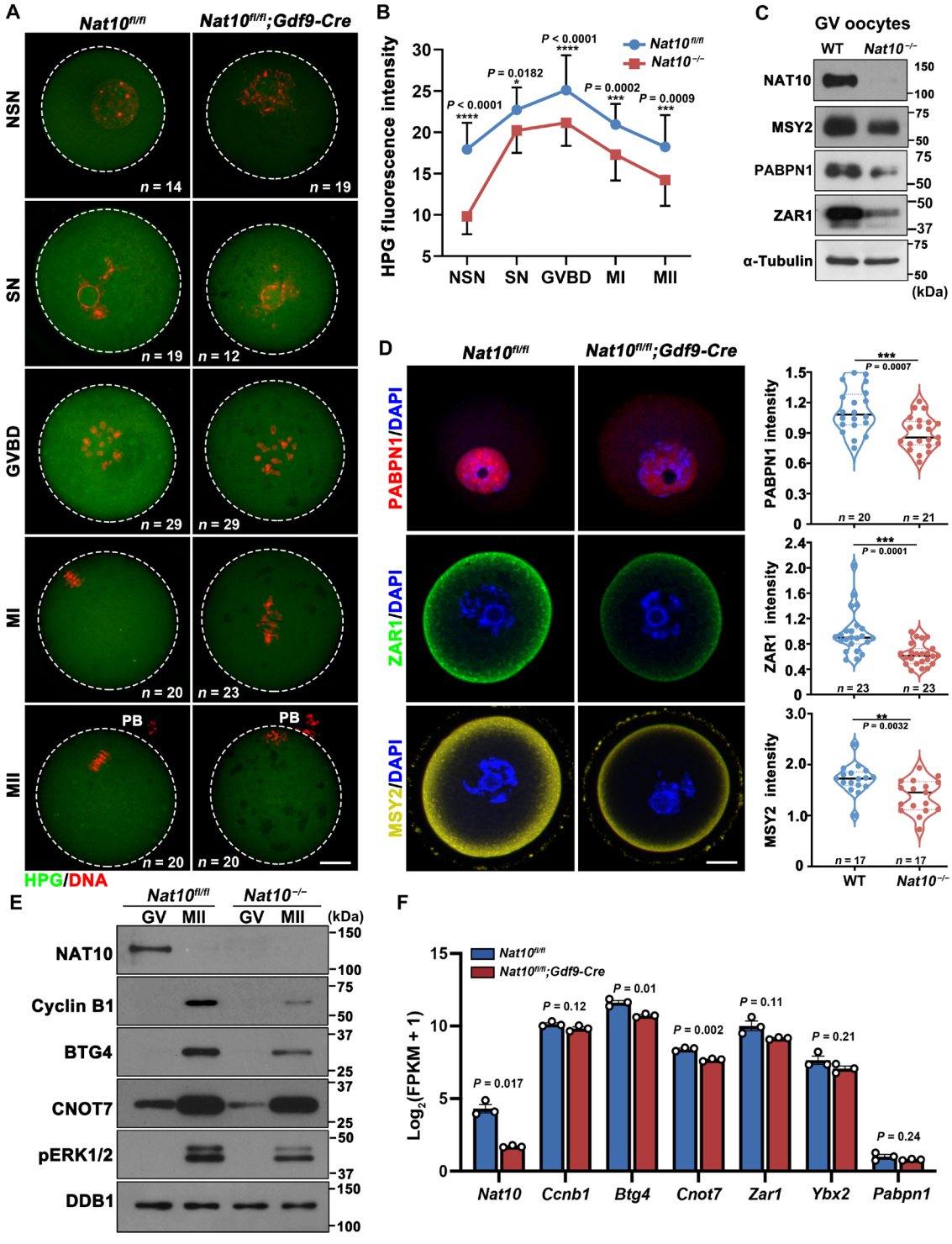

Fig. 7. *Nat10* deletion affects mRNA translation efficiency during oocyte maturation. (**A**) The Click-iT HPG Alexa Fluor 488 protein synthesis assay detects changes in overall translation levels during oocyte meiotic maturation. (**B**) Quantitative statistics of HPG fluorescence signals in (A). (**C**) Western blot results showing the levels of the indicated proteins in WT and *Nat10*-deleted GV oocytes. Total proteins of 100 oocytes in each lane. (**D**) Immunofluorescence and quantification results of the indicated proteins in WT and *Nat10*-deleted GV oocytes. (**E**) Western blot results showing levels of the indicated proteins in WT and *Nat10*-deleted oocytes before and after meiotic maturation. Total proteins of 100 oocytes in each lane. (**F**) RNA-seq results showing the mRNA levels of indicated genes in WT and *Nat10*-deleted oocytes at the GV stage. Scale bars, 20 μm for all panels in (A) and (D).

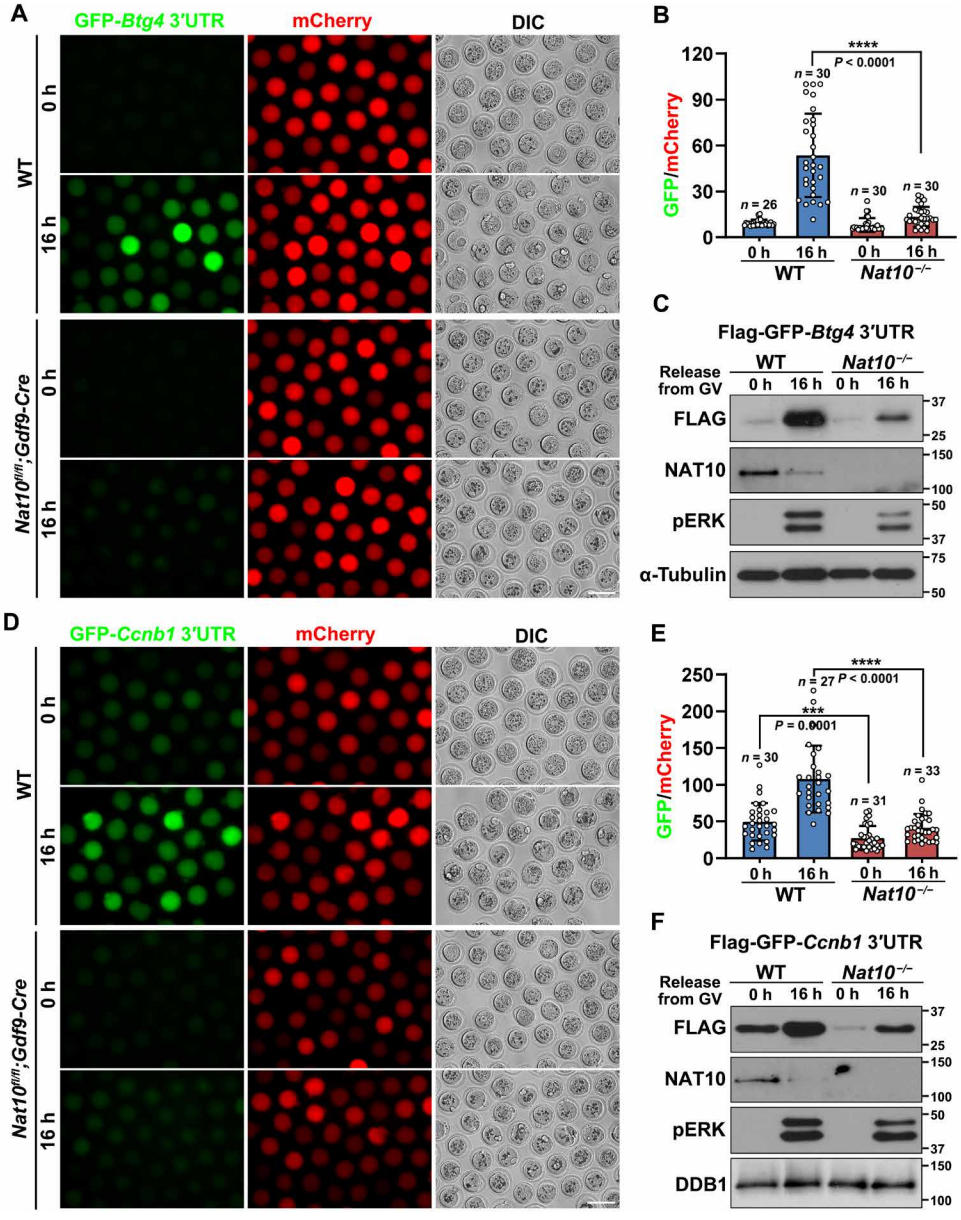

Fig. 8. Reduced translational activation of key maternal mRNAs in *Nat10*-deleted oocytes. (**A**) GFP-*Btg4* 3′UTR reporter assay detects *Btg4* mRNA translation efficiency during oocyte maturation in WT and *Nat10*$^{fl/fl}$;*Gdf9-Cre* mice. (**B**) Quantification of GFP/mCherry fluorescence intensity. (**C**) Western blotting to detect the translational activity of *Btg4* 3′UTR during oocyte maturation of WT and *Nat10*$^{fl/fl}$;*Gdf9-Cre* mice. The Flag protein level indicates the translation activity of the reporter plasmid. (**D**) GFP-*Ccnb1* 3′UTR reporter assay detects *Ccnb1* mRNA translation efficiency during oocyte maturation in WT and *Nat10*$^{fl/fl}$;*Gdf9-Cre* mice. (**E**) Quantification of GFP/mCherry fluorescence intensity. (**F**) Western blotting to detect the translational activity of *Ccbn1* 3′UTR during oocyte maturation of WT and *Nat10*$^{fl/fl}$;*Gdf9-Cre* mice. Scale bars, 100 μm for all panels in (A) and (D).

where the modification occurred at a single-nucleotide resolution. In contrast, ac^{4}C-seq is a single-nucleotide resolution approach that relies on chemical treatment to change the physicochemical properties of modified bases, resulting in mismatches during the subsequent reverse transcription of library construction (*16*, *25*). However, this approach is limited to detecting low stoichiometric bases in mRNAs expressed at low levels. This method also requires a deeper sequencing depth; otherwise, it is difficult to fully reflect the actual stoichiometric sites and the abundance of modifications.

Despite the controversy in the field, we attempted to provide strengthened evidence to support our main conclusions in this study: (i) First, NAT10 is the only known ac^{4}C writer protein that can directly or indirectly capture RNA-containing ac^{4}C peaks under physiological conditions. In this study, we used ac^{4}C and NAT10 antibodies to carry out LACE-seq (Fig. 2). Our results showed that the peaks captured by the two antibodies and the distribution patterns were highly similar, and more than 50% of NAT10 binding peaks overlapped with ac^{4}C peaks (Fig. 3 and fig. S2), validating the repeatability and reliability of the ac^{4}C peaks in our study. (ii) We also set up IgG controls and *Nat10*-null oocytes as negative controls. Our results showed that the ac^{4}C peaks identified in WT oocytes were significantly reduced or eliminated after the deletion of *Nat10* (Fig. 5), indicating that the ac^{4}C

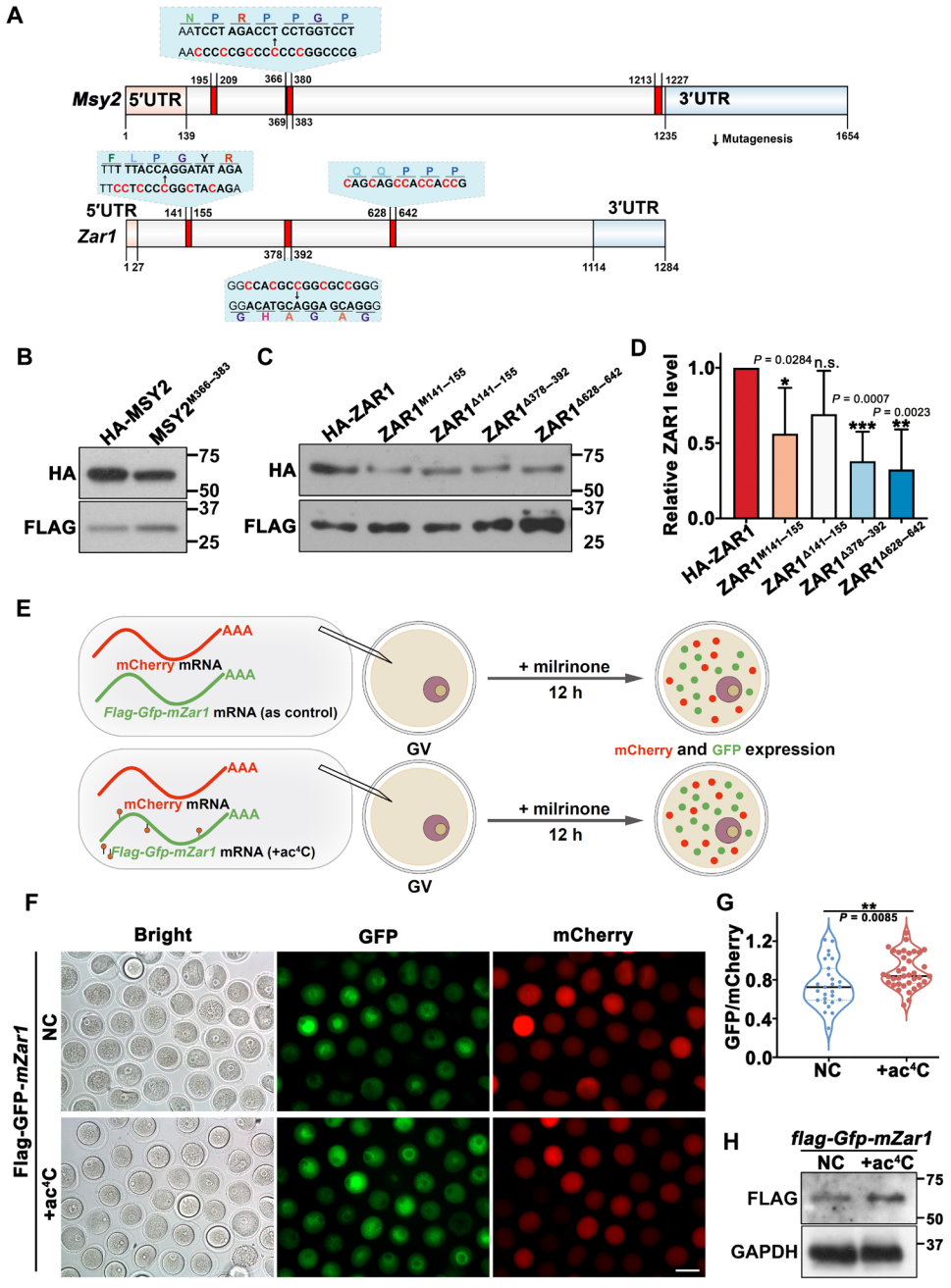

Fig. 9. Effects of mRNA ac^{4}C modifications on the translation of key mRNAs in oocytes. (**A**) Localization of ac^{4}C modification sites in the encoding regions of *Msy2* and *Zar1* transcripts predicted by PACES software. Selected ac^{4}C sites were mutated without affecting the amino acids. (**B** and **C**) Western blotting results showing protein expression levels of MSY2 and ZAR1 before and after mutations of ac^{4}C sites. Human embryonic kidney 293T cells (RRID: CVCL_0063) were transfected with plasmids encoding WT and ac^{4}C site–mutated *Msy2* and *Zar1* cDNAs. (**D**) Quantifications of the band intensities in (C). (**E**) Illustration of in vitro transcription and oocyte microinjection of *Zar1* mRNAs with or without ac^{4}C incorporation. (**F**) Fluorescence results show the expression of *Zar1* mRNAs with or without enhanced ac^{4}C modifications by ac^{4}CTP incorporation in GV oocytes at 24 hours after microinjections. mRNAs encoding mCherry were co-injected as an internal control. Scale bar, 100 μm. (**G**) Quantifications of relative GFP/mCherry intensities in (F). (**H**) Western blotting results showing expression levels of FLAG-GFP-ZAR1 proteins from *Zar1* mRNAs with or without enhanced ac^{4}C modifications.

peaks identified in WT oocytes are highly dependent on NAT10. We also observed that the ac^{4}C signal was significantly reduced in *Nat10*-null oocytes using immunofluorescence staining results (Fig. 1, F and G). These results are equally convincing, as previous studies have shown that overexpression of exogenous "NAT10-THUMPD1" can induce increased ac^{4}C signals (*16*).

In addition, compared with previous studies that relied heavily on bioinformatics analysis to draw conclusions, the physiological phenotypes of oocyte meiotic defects are highly consistent with the known biochemical mechanism that ac^{4}C modification can promote translation efficiency in our study. When *Nat10* was lost, the overall ac^{4}C modification level was significantly reduced (Fig. 5),

dampening the translation efficiency of key proteins and ultimately leading to defects in oocyte meiotic maturation (Figs. 6 to 9). We also constructed *Btg4* and *Ccnb1* translation reporter plasmids for further verification, which significantly reduced the ac^{4}C signal and played an essential role in oocyte maturation. We found that the translation activities of *Btg4* and *Ccnb1* reporters were reduced considerably during meiosis in *Nat10*-null oocytes (Fig. 8). We also constructed synonymous mutations in the ac^{4}C modification sites of *Msy2* and *Zar1* and found that the translational activities of *Msy2* and *Zar1* were significantly reduced after mutation of the ac^{4}C sites (Fig. 9, A to D). Our constructed reporter plasmid artificially enhanced the stoichiometry of the ac^{4}C modification of *Zar1* mRNA by in vitro transcription, and the translation activity of the *Zar1* + ac^{4}C reporter plasmid was significantly increased (Fig. 9, E to H). The above loss- and gain-of-function experiments and significant physiological phenotypes strongly support the idea that ac^{4}C modification ensures the completion of oocyte meiotic maturation by enhancing translation efficiency.

The use of antibodies to detect RNA modifications is a well-recognized method in this field that has been widely used in studies of m^{6}A modification detection. Although the specificity of ac^{4}C antibodies has been fully verified in previous studies (*22*, *23*), some studies still doubt the specificity of ac^{4}C antibodies and the reliability of methods using these antibodies to detect ac^{4}C modifications (*41*). The above evidence revealed that the ac^{4}C signal detected in this study was highly dependent on NAT10. Here, we present another antibody-independent ac^{4}C modification detection method that supports our conclusions. In a previous study, liquid chromatography–tandem mass spectrometry was used to detect changes in ac^{4}C modification of poly(A) RNA. The results showed that the stoichiometry of the ac^{4}C modification of poly(A) RNA in NAT10$^{-/-}$ HeLa cells was significantly reduced compared to that in the WT (*15*). In addition, a study previously published by our team used liquid chromatography–tandem mass spectrometry to show that the abundance of ac^{4}C modification in mRNA from the testes of *Nat10*$^{fl/-}$*;Stra8-Cre* mice was significantly reduced (*17*). These two studies used ac^{4}C antibody–independent detection technologies that showed the presence of ac^{4}C modification in WT HeLa cells and mouse testis mRNA. These ac^{4}C signals were highly dependent on NAT10, strongly supporting the conclusions of our study.

To verify the ac^{4}C LACE-seq method, we also performed LACE-seq of NAT10. NAT10 is the only ac^{4}C writer protein currently known. Although NAT10 contains a tRNA-binding domain (*43*), it has not been reported to bind mRNAs directly. The ac^{4}C peaks captured by NAT10 are presumed to bind with NAT10 indirectly through its "Adaptor" proteins. To date, RBPs that mediate ac^{4}C modifications in mRNAs remain elusive. In our study, the ac^{4}C peaks captured by both ac^{4}C LACE-seq and NAT10 LACE-seq showed higher signal intensities, indicating the credibility of the ac^{4}C peaks. Many ac^{4}C peaks were captured by ac^{4}C LACE-seq than by NAT10 LACE-seq. A likely explanation is that the transcripts dissociated from NAT10 after ac^{4}C establishment.

Previously, ac^{4}C-related research was limited to the application of low-input detection technologies. In this study, we developed an ac^{4}C LACE-seq, which is suitable for a small number of samples. This technology has the advantages of high sensitivity and low input compared with other published ac^{4}C detection technologies. The development of this technology will help promote ac^{4}C-related research in germ cells and early embryonic development, as well as benefit other fields. In addition, the development of ac^{4}C LACE-seq technology will provide inspiration and a paradigm for developing other mRNA modification detection technologies, arousing widespread interest in epitranscriptomics.

Using oocyte-specific *Nat10* knockout mice as a model, this study confirmed that ac^{4}C modification of mRNA in oocytes is catalyzed by NAT10 and that NAT10-mediated ac^{4}C modification has critical physiological functions during meiotic maturation and female fertility (Fig. 10). Transcriptome analyses indicated that ac^{4}C modification in oocytes is highly coupled to translation efficiency rather than affecting transcript stability and that ac^{4}C drives precise regulation of the oocyte meiotic maturation process by enhancing translation efficiency (Fig. 9). In addition to mRNAs, ac^{4}C modifications were detected in the tRNAs of leucine and serine and at two sites on the 18S rRNA. We also observed high levels of ac^{4}C signals in the nuclear-like bodies of GV oocytes and zygotes, where rRNA was enriched. When *Nat10* was deleted, these nucleolar ac^{4}C signals disappeared, confirming that NAT10 was responsible for rRNA ac^{4}C modifications in mouse oocytes. It is conceivable that NAT10-mediated ac^{4}C modifications of mRNAs, tRNAs, and 18S rRNAs contribute to efficient mRNA translation activity in oocytes. Studies in yeast and cultured mammalian cell lines have shown that the disruption of ac^{4}C modifications on tRNAs (tRNA-Ser and tRNA-Leu) and 18S rRNAs delayed the cell growth rate but did not cause cell death, suggesting that ac^{4}C modifications on tRNAs and 18S rRNAs facilitate mRNA translation but are not essential (*13*, *15*, *34*–*36*, *44*). This observation was consistent with the limited distribution of ac^{4}C modifications in tRNAs and 18S rRNAs. In contrast, we provide experimental evidence that ac^{4}C modifications of key maternal mRNAs positively regulate their translational efficiencies. We propose that NAT10-mediated ac^{4}C modifications in all three types of RNAs, including mRNAs encoding key maternal factors, are crucial for efficient maternal mRNA translation during mouse oocyte maturation (Fig. 10).

In addition to causing mRNA translation defects, *Nat10* deletion also influenced the levels of specific transcripts in oocytes, as shown in our study and a recent report (*38*). ac^{4}C modifications may directly affect the stability of some mRNAs; however, the underlying mechanisms remain unknown. In our opinion, *Nat10* deletion in oocytes is likely to affect transcript stability via the following indirect mechanisms: (i) There was compromised translation of mRNAs encoding key maternal factors involved in transcript storage, particularly MSY2 and ZAR1. Previous studies have shown that *Msy2* or *Zar1* knockout leads to premature decay of maternal mRNAs and defects in oocyte maturation. (ii) Impaired translational activation of transcripts encoding proteins responsible for mRNA degradation, such as BTG4 and CNOT7, was reported in this study and recently reported (*38*). (iii) Ribosome binding and active translation of transcripts also play a role in mRNA stability in mouse oocytes and zygotes. Therefore, ac^{4}C modification may indirectly affect the stability of maternal mRNAs by regulating their translation efficiency.

We acknowledge the limitations of this study. We have not yet mapped the dynamic changes in ac^{4}C modification during the entire meiotic maturation process and preimplantation embryonic development. We attempted to identify ac^{4}C-modified mRNAs in MII oocytes and zygotes using the ac^{4}C LACE-seq method without success. Maternal mRNAs undergo extensive degradation during meiotic maturation and fertilization (*45*, *46*). However, de novo transcription

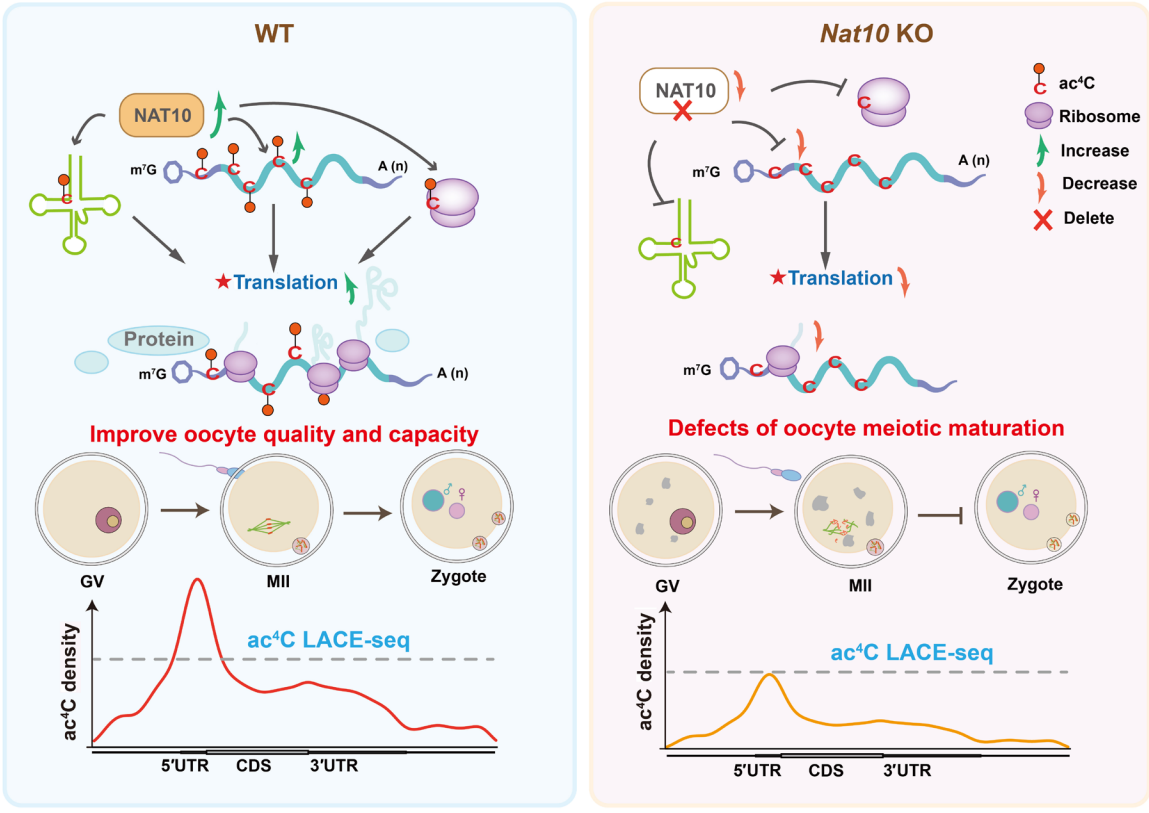

Fig. 10. Schematic diagram of NAT10-mediated mRNA N^4-acetylcytidine regulates translation of key proteins during oocyte meiotic maturation. In WT mice, NAT10 catalyzes ac^{4}C modification on mRNA, tRNAs, and rRNAs and promotes the timely translation of proteins from these key transcripts to ensure normal oocyte meiotic maturation. When NAT10 is absent, the RNA ac^{4}C modification cannot be established, and the translation efficiency of these transcripts is reduced, leading to defects in the meiotic maturation process, ultimately leading to infertility in female mice.

did not occur during this process. Therefore, it is possible that the levels of ac^{4}C-modified maternal mRNAs at these developmental stages were too low to be effectively detected using the ac^{4}C LACE-seq method.

Now, the mechanisms through which mRNA ac^{4}C modifications facilitate translation are unknown. Studies in cultured somatic cells have suggested that ac^{4}C modifications increase the binding efficiency of transcripts to ribosomes, especially at the wobbled third base of codons (*13*, *15*, *47*). Interactions between mRNA ac^{4}C modification sites and key RBPs, particularly those involved in the translational regulation of oocytes, remain to be investigated.

MATERIALS AND METHODS

Animals

All experiments involving mouse strains used in this study involved a C57BL/6J genetic background. The *Gdf9-Cre* transgenic mouse line has been previously described (*48*). *Nat10*-floxed mice (*Nat10* $^{flox/flox}$) in which exons 2 and 3 were flanked with sites, as previously reported (*17*), were crossed with the *Gdf9-Cre* mouse line to generate *Nat10* conditional knockout mice. Mice were housed in cages under the specific pathogen–free environment of the Laboratory Animal Center of Zhejiang University, which was controlled at 50 to 70% humidity and a 12/12-hour light/dark cycle with 20° to 22°C temperature and water and food provided ad libitum. Animal experiment use and care were performed in compliance with the regulations and guidelines of Zhejiang University. The experimental procedures were approved by the Institutional Animal Care and Research Committee of Zhejiang University (approval no. ZJU20210252 to H.-Y.F.). The primers used for genotyping are listed in table S14.

Superovulation and fertilization

For superovulation, female mice (28 to 35 days of age) were intraperitoneally injected with 5 IU of pregnant mare serum gonadotropin (PMSG; Ningbo Sansheng Pharmaceutical). After 44 hours, the ovaries were punctured with needles to collect GV oocytes or the mice were injected with 5 IU of human chorionic gonadotropin (hCG; Ningbo Sansheng Pharmaceutical). After an additional 16 hours, the cumulus-oocyte complex masses were surgically removed from the oviducts, and MII oocytes were collected by digestion with 0.3% hyaluronidase (Sigma-Aldrich). The oocyte morphology was observed, and images were acquired using a Nikon SMZ1500 stereoscope. To collect early embryos, 4-week-old female mice were mated with adult WT males immediately after hCG injection. The presence of vaginal plugs confirmed successful mating. Embryos were harvested from the oviducts after hCG injection at the indicated time points.

Mouse oocyte and embryo in vitro culture and collection

Fully grown oocytes were harvested from female mice at 28 to 35 days of age that were superovulated 44 hours later by injection of 5 IU of

PMSG in 37°C prewarmed M2 medium (M7167; Sigma-Aldrich) and cultured in M16 medium (M7292; Sigma-Aldrich) covered with mineral oil (M5310; Sigma-Aldrich). Mice at 28 days of age were superovulated, fertilized with adult WT males, and inspected for the presence of vaginal plugs 20 hours after hCG injection. In some experiments, the obtained embryos were further cultured at 37°C with a 5% CO_2 atmosphere in KSOM medium (Millipore, MR-106-D).

Preparation of mRNA for microinjections

The expression vectors were linearized and in vitro transcribed to prepare mRNA for microinjection using the SP6 message mMACHINE Kit (Invitrogen, AM1340). Poly(A) tails [~200 to 250 base pairs (bp)] were added to the transcribed mRNAs using a mMACHINE kit (Invitrogen, AM1350). The in vitro–transcribed mRNAs were recovered using lithium chloride precipitation and resuspended in nuclease-free water. The concentration of all injected RNAs was adjusted to 500 ng/μl. To add ac^4C to the transcription products, N^4-acetyl-CTP (N^4-acetyl-cytidine-5′-*O*-triphosphate) and CTP were added to the in vitro transcription reactions at 1:10 according to the instruction manuals of High Yield T7 Cap 1 AG (3′-OMe) mRNA Synthesis Kit (ac^4CTP) (Jena Bioscience, RNT-128-L).

Microinjection of oocytes

Fully grown oocytes at the GV stage were incubated in an M2 medium containing 2 μM milrinone to inhibit spontaneous GVBD for later microinjection. All injections were administered using an Eppendorf Transferman NK2 micromanipulator. RNA (~5 to 10 pl) at a concentration of 500 ng/μl was microinjected into each oocyte. After microinjection, oocytes were cultured in M16 medium with (arrested at the GV stage) or without (released to undergo meiotic resumption) 2 μM milrinone at 37°C and 5% CO_2.

Immunofluorescence and confocal microscopy

For immunofluorescence staining, oocytes or embryos were fixed at the indicated time points in phosphate-buffered saline (PBS)–buffered 4% paraformaldehyde for 30 min at room temperature and subsequently transferred to PBS-buffered 0.3% Triton X-100 for 15 min for permeabilization. We used 1% paraformaldehyde and 0.5% Triton X-100 for simultaneous fixation and permeabilization on ice for 1 hour to detect nuclear protein or nuclear localization signal. After blocking in PBS-buffered 1% bovine serum albumin, oocytes were incubated with primary antibodies diluted in blocking solution at room temperature for 1 hour or 4°C overnight. Oocytes were washed thrice in PBS, probed at room temperature with secondary antibodies for 30 min, and counterstained with 4′,6-diamidino-2-phenylin-dole (DAPI; 5 μg/ml) or propidium iodide (Molecular Probes, Life Technologies) for 10 min. Last, the oocytes were washed and mounted on glass slides using SlowFade Gold Antifade Reagent (Life Technologies). Imaging of the oocytes or embryos after immunofluorescence was performed using a Zeiss LSM710 confocal microscope. The antibodies used in this study are listed in table S15. Semiquantitative analysis of the fluorescence signals was performed using ImageJ software.

Detection of protein synthesis in embryos

To detect nascent protein synthesis, two-cell-stage embryos of WT and *Nat10*$^{fl/fl}$;*Gdf9-Cre* were cultured in KSOM medium supplemented with 50 μM HPG from Click-iT HPG Alexa Fluor protein synthesis assay kits (Thermo Fisher Scientific) for 2 hours. After washing thrice with PBS, the embryos were fixed in 4% formaldehyde for 30 min at room temperature. After permeabilization and washing according to previously described standard protocols, Alexa Fluor 488 was conjugated to the protein using a Click-iT cell reaction kit, and DAPI was counterstained. The fluorescence signal was subtracted from the background and measured and quantified using ImageJ software.

Histological analysis and immunohistochemistry

Freshly isolated ovary samples extracted from WT and *Nat10*$^{fl/fl}$;*Gdf9-Cre* female mice were collected and fixed overnight in PBS-buffered formalin at 4°C, dehydrated, processed, and embedded in paraffin using standard protocols. Ovaries were serially sectioned 5 mm thick and stained with hematoxylin and eosin following standard protocols. For immunohistochemistry staining, sections were deparaffinized and rehydrated. The slides were then incubated in 3% H_2O_2 (v/v) for 10 min at room temperature, boiled for 15 min in 10 mM sodium citrate buffer (pH 6.0), and incubated in a blocking buffer containing 10% donkey serum for 40 min at 25°C. Primary antibodies were applied at suitable dilutions at 4°C overnight, and samples were washed three times with PBS with Tween 20 for 10 min each time and incubated with biotinylated secondary antibodies for 30 min at room temperature. After several washes in PBS with Tween 20, the sections were stained using Vectastain ABC and DAB peroxidase substrate kits (Vector Laboratories). Last, the slides were counterstained with hematoxylin before mounting. The sections were imaged using a bright-field microscope. The antibodies used in this study are listed in table S15.

Western immunoblotting analysis

Protein samples of oocytes or embryos were lysed and denatured in 2× SDS sample buffer containing β-mercaptoethanol for total protein extraction and heated for 15 min at 95°C. Proteins were separated using SDS–polyacrylamide gel electrophoresis and electrophoretically blotted onto microporous polyvinylidene fluoride membranes (Millipore) under a constant current. Membranes containing the transferred proteins were rinsed and blocked in 0.1% Tween 20 in tris-buffered saline (TBST) containing 5% nonfat milk (BD Biosciences) at room temperature for 1 hour. After being probed with primary antibodies at a predetermined concentration overnight at 4°C, the membranes were washed three times in TBST for 15 min, incubated with the corresponding horseradish peroxidase–linked secondary antibody (Jackson ImmunoResearch Laboratories) for 40 min at room temperature, and subsequently washed three times with TBST. Last, the exposed bound signals were detected using an enhanced chemiluminescence Western blotting substrate (Thermo Fisher Scientific, 32106) or SuperSignal West Femto maximum sensitivity substrate (Thermo Fisher Scientific). The antibodies used in this study are listed in table S15, and all the unprocessed gel figures are shown in fig. S5.

RNA isolation and real-time RT-PCR

Five oocytes or embryos were collected and lysed in 2 μl of lysis buffer (0.2% Triton X-100 and 4 IU of ribonuclease inhibitor), and cDNA synthesis was followed by retrotranscribing reverse transcription with primer transcript II reverse transcriptase (Takara) according to the manufacturer's protocol. RT-qPCR analysis was performed using Power SYBR Green PCR Master Mix (Applied Biosystems, Life Technologies) and an Applied Biosystems ABI 7500 Real-Time PCR system using the primers listed in table S14. Relative mRNA expression levels were calculated to the levels of endogenous glyceraldehyde

3-phosphate dehydrogenase mRNA (used as a housekeeping gene) using Microsoft Excel, and each RT-qPCR experimental reaction was performed in triplicate.

LACE-seq

The NAT10 LACE-seq experiments were performed according to a previously published protocol (*26*). IgG treatment was consistent with NAT10 LACE-seq in this study. For ac^4C LACE-seq, oocyte samples were incubated with ac^4C antibodies first, followed by UV cross-linking to cross-link ac^4C antibodies with RNA-containing ac^4C in cells to produce a steric hindrance effect. The subsequent steps are carried out according to LACE-seq (*26*). Briefly, 50 oocytes were collected in 1.5-ml Eppendorf LoBind microcentrifuge tubes and quickly spun down to the bottom with a minicentrifuge. Samples were lysed on ice using 50 μl of wash buffer for 10 min. Next, 1 μl of ribonuclease inhibitor (Ambion, AM2696) and 4 μl of RQ1 deoxyribonuclease (Promega, M6101) were applied to the lysate and incubated at 37°C for 3 min. After snap-chilling the tube on ice for 3 min, 2 μg of antibody was added, and the tube was rotated at 4°C for 1 hour. Next, the samples were irradiated twice with UV-C light on the ice at 400 mJ, and then 10 μl of protein A/G beads was added to the sample and rotated for 2 hours at 4°C. After extensive washing steps, the immunoprecipitated RNA was fragmented and experienced 3′-dephosphorylation and linker ligation, followed by reverse transcription on beads. Then, first-strand cDNAs were derived from protein A/G beads and further captured by streptavidin C1 beads for pre-PCR, and a 3′-cDNA linker was added to produce double-stranded DNA as the template for in vitro transcription. In vitro transcription products were purified by removing the DNA template using Turbo deoxyribonuclease and further purified using Agencourt RNA Clean beads according to the manufacturer's instructions. The linearly amplified RNA was then transformed into cDNA and amplified using PCR using P7 and barcoded P5 index primers. Final PCR products of 250 to 500 bp were excised from a 2% agarose gel and purified using a gel purification kit (Qiagen, catalog no. 28604) according to the manufacturer's instructions.

LACE-seq data mapping

Adapter sequences and low-quality bases of the raw reads were removed using Trim-Galore (version 0.6.7) with the following parameters: --clip_R2 10 --clip_R1 10 --three_prime_clip_R1 4 --three_prime_clip_R2 4 --paired --phred33 --trim-n --stringency 3 --length 25 --fastqc. Clean reads were first aligned to mouse pre-rRNA using Bowtie software (version 2.3.5.1) (*49*), and the remaining unmapped reads were then aligned to the mouse (mm10) reference genome using hisat2 (version 2.2.1) (*50*). For LACE-seq data mapping, two mismatches were allowed (Bowtie parameters: --sensitive-local -N 1 --local --no-mixed --un-conc-gz -p 30 -x reference genome -1 -2; Hisat2 parameters: -k 1 --no-discordant -p 30 --dta-cufflinks -x reference genome -1 -2). Then, the PCR duplicates were removed using Sambamba (version 0.7.1) (*51*). The correlation between LACE-seq replicates was calculated as follows: The LACE-seq correlation was calculated using the deepTools (version 3.5.1) "plotCorrelation" function with the parameters –corMethod spearman --colorMap bwr --plotNumbers -p heatmap and then using deepTools bamcoverage with default parameters to generate bigwig files for visualization (*52*).

LACE-seq peak and motif identification

MACS (version 2.2.7.1) software was used to identify peaks in WT and *Nat10* knockout oocytes. The parameters were as follows: --keep-dup all --fe-cutoff 2 -p 0.001 --extsize 100 –nomodel (*53*). Only peaks that appeared in both replicates were retained. For motif analysis, LACE-seq peaks were first extended 30 nucleotides to 5′ upstream, and its corresponding sequence on the mm10 reference genome was obtained using bedtools (version 2.30.0) with the following parameters: -fi -bed -fo (*54*). Then, Meme (version 4.11.2) software obtained their motif logo with default parameters.

RNA-seq library preparation

For RNA-seq library construction, three replicates of zygote and two-cell stage samples (10 embryos per sample) were collected from WT and *Nat10*$^{fl/fl}$;*Gdf9-Cre* mice. Embryonic mRNA extraction and reverse transcription were performed using the Smart-seq2 protocol as previously described. Briefly, 4-week-old female mice were injected with hCG 44 hours after PMSG injection and mated with WT male mice. Embryos were collected 20 hours later in vivo. Each sample was directly lysed in 4 μl of lysis buffer [including 0.2 μl of 1:1000 diluted External RNA Controls Consortium (ERCC) spike-in] and immediately reverse transcribed using the PrimeScript II Reverse Transcriptase (Takara, catalog no. 2690A), and the cDNA library was constructed as the published Smart-seq2 method. Raw reads were sequenced using the Illumina NovaSeq 6000 platform in the 151-bp paired-end mode.

RNA-seq data analysis

Raw reads were trimmed with Trim-Galore (version 0.6.7) and mapped to the mm10 genome using STAR (version 2.7.10a). Uniquely mapped reads were used to quantify gene expression using Feature Counts (version 2.0.2) and further normalized to the ERCC spike-in. The ERCC table was obtained as described above using the ERCC reference genome, and the percentage of ERCC reads was used for data calibration. Differential gene expression analysis was performed using the DESeq2 R package, and adjusted $P < 0.05$ and absolute $\log_2$(FC of *Nat10*-null/WT) > 1 were used as statistical significance to identify DEGs (table S12). Transcripts per million were calculated to estimate gene expression levels, normalized to gene length and sequencing depth. ERCC-calibrated counts and transcripts per million are listed in table S11.

Statistical analysis

The experiments were randomized and performed by blinding the experimental conditions. No statistical method was used to predetermine the sample size. Informed consent was obtained from all the subjects. Results are given as means ± SEM. Each experiment included at least three independent samples and was repeated at least three times. The results of the two experimental groups were compared using two-tailed unpaired Student's *t* tests. Statistically significant values were $^*P < 0.05$, $^{**}P < 0.01$, $^{***}P < 0.001$, and $^{****}P < 0.0001$.

Supplementary Materials

The PDF file includes:

Figs. S1 to S5

Legends for tables S1 to S15

Other Supplementary Material for this manuscript includes the following:

Tables S1 to S15

REFERENCES AND NOTES

1. M. Christou-Kent, M. Dhellemmes, E. Lambert, P. F. Ray, C. Arnoult, Diversity of RNA-binding proteins modulating post-transcriptional regulation of protein expression in the maturing mammalian oocyte. *Cells* **9**, 662 (2020).

2. J. M. Reyes, P. J. Ross, Cytoplasmic polyadenylation in mammalian oocyte maturation. *Wiley Interdiscip. Rev. RNA* **7**, 71–89 (2016).
3. A. Susor, D. Jansova, M. Anger, M. Kubelka, Translation in the mammalian oocyte in space and time. *Cell Tissue Res.* **363**, 69–84 (2016).
4. A. Susor, D. Jansova, R. Cerna, A. Danylevska, M. Anger, T. Toralova, R. Malik, J. Supolikova, M. S. Cook, J. S. Oh, M. Kubelka, Temporal and spatial regulation of translation in the mammalian oocyte via the mTOR-eIF4F pathway. *Nat. Commun.* **6**, 6078 (2015).
5. I. A. Roundtree, M. E. Evans, T. Pan, C. He, Dynamic RNA modifications in gene expression regulation. *Cell* **169**, 1187–1200 (2017).
6. P. Boccaletto, F. Stefaniak, A. Ray, A. Cappannini, S. Mukherjee, E. Purta, M. Kurkowska, N. Shirvanizadeh, E. Destefanis, P. Groza, G. Avsar, A. Romitelli, P. Pir, E. Dassi, S. G. Conticello, F. Aguilo, J. M. Bujnicki, MODOMICS: A database of RNA modification pathways. 2021 update. *Nucleic Acids Res.* **50**, D231–D235 (2022).
7. F. Morena, C. Argentati, M. Bazzucchi, C. Emiliani, S. Martino, Above the epitranscriptome: RNA modifications and stem cell identity. *Genes* **9**, 329 (2018).
8. P. C. He, C. He, mRNA acetylation: A new addition to the epitranscriptome. *Cell Res.* **29**, 91–92 (2019).
9. H. G. Zachau, D. Dütting, H. Feldmann, The structures of two serine transfer ribonucleic acids. *Hoppe Seylers Z. Physiol. Chem.* **347**, 212–235 (1966).
10. S. Kowalski, T. Yamane, J. R. Fresco, Nucleotide sequence of the "denaturable" leucine transfer RNA from yeast. *Science* **172**, 385–387 (1971).
11. Z. Oashi, K. Murao, T. Yahagi, D. L. Von Minden, J. A. McCloskey, S. Nishimura, Characterization of C^+ located in the first position of the anticodon of *Escherichia coli* $tRNA^{Met}$ as N^4-acetylcytidine. *Biochim. Biophys. Acta* **262**, 209–213 (1972).
12. L. Stern, L. H. Schulman, The role of the minor base N^4-acetylcytidine in the function of the *Escherichia coli* noninitiator methionine transfer RNA. *J. Biol. Chem.* **253**, 6132–6139 (1978).
13. T. Taniguchi, K. Miyauchi, Y. Sakaguchi, S. Yamashita, A. Soma, K. Tomita, T. Suzuki, Acetate-dependent tRNA acetylation required for decoding fidelity in protein synthesis. *Nat. Chem. Biol.* **14**, 1010–1020 (2018).
14. G. Thomas, J. Gordon, H. Rogg, N^4-Acetylcytidine. A previously unidentified labile component of the small subunit of eukaryotic ribosomes. *J. Biol. Chem.* **253**, 1101–1105 (1978).
15. D. Arango, D. Sturgill, N. Alhusaini, A. A. Dillman, T. J. Sweet, G. Hanson, M. Hosogane, W. R. Sinclair, K. K. Nanan, M. D. Mandler, S. D. Fox, T. T. Zengeya, T. Andresson, J. L. Meier, J. Coller, S. Oberdoerffer, Acetylation of cytidine in mRNA promotes translation efficiency. *Cell* **175**, 1872–1886.e24 (2018).
16. A. Sas-Chen, J. M. Thomas, D. Matzov, M. Taoka, K. D. Nance, R. Nir, K. M. Bryson, R. Shachar, G. L. S. Liman, B. W. Burkhart, S. T. Gamage, Y. Nobe, C. A. Briney, M. J. Levy, R. T. Fuchs, G. B. Robb, J. Hartmann, S. Sharma, Q. Lin, L. Florens, M. P. Washburn, T. Isobe, T. J. Santangelo, M. Shalev-Benami, J. L. Meier, S. Schwartz, Dynamic RNA acetylation revealed by quantitative cross-evolutionary mapping. *Nature* **583**, 638–643 (2020).
17. L. Chen, W.-J. Wang, Q. Liu, Y.-K. Wu, Y.-W. Wu, Y. Jiang, X.-Q. Liao, F. Huang, Y. Li, L. Shen, C. Yu, S.-Y. Zhang, L.-Y. Yan, J. Qiao, Q.-Q. Sha, H.-Y. Fan, NAT10-mediated N^4-acetylcytidine modification is required for meiosis entry and progression in male germ cells. *Nucleic Acids Res.* **50**, 10896–10913 (2022).
18. T. Niwa, N. Takeda, H. Yoshizumi, RNA metabolism in uremic patients: Accumulation of modified ribonucleosides in uremic serum. Technical note. *Kidney Int.* **53**, 1801–1806 (1998).
19. C. L. Parsons, T. Shaw, Z. Berecz, Y. Su, P. Zupkas, S. Argade, Role of urinary cations in the aetiology of bladder symptoms and interstitial cystitis. *BJU Int.* **114**, 286–293 (2014).
20. H. Li, Q. Qin, X. Shi, J. He, G. Xu, Modified metabolites mapping by liquid chromatography-high resolution mass spectrometry using full scan/all ion fragmentation/neutral loss acquisition. *J. Chromatogr. A* **1583**, 80–87 (2019).
21. E. Szymańska, M. J. Markuszewski, M. Markuszewski, R. Kaliszan, Altered levels of nucleoside metabolite profiles in urogenital tract cancer measured by capillary electrophoresis. *J. Pharm. Biomed. Anal.* **53**, 1305–1312 (2010).
22. W. R. Sinclair, D. Arango, J. H. Shrimp, T. T. Zengeya, J. M. Thomas, D. C. Montgomery, S. D. Fox, T. Andresson, S. Oberdoerffer, J. L. Meier, Profiling cytidine acetylation with specific affinity and reactivity. *ACS Chem. Biol.* **12**, 2922–2926 (2017).
23. J. M. Thomas, C. A. Briney, K. D. Nance, J. E. Lopez, A. L. Thorpe, S. D. Fox, M. L. Bortolin-Cavaille, A. Sas-Chen, D. Arango, S. Oberdoerffer, J. Cavaille, T. Andresson, J. L. Meier, A chemical signature for cytidine acetylation in RNA. *J. Am. Chem. Soc.* **140**, 12667–12670 (2018).
24. J. M. Thomas, K. M. Bryson, J. L. Meier, Nucleotide resolution sequencing of N4-acetylcytidine in RNA. *Methods Enzymol.* **621**, 31–51 (2019).
25. S. Thalalla Gamage, A. Sas-Chen, S. Schwartz, J. L. Meier, Quantitative nucleotide resolution profiling of RNA cytidine acetylation by ac4C-seq. *Nat. Protoc.* **16**, 2286–2307 (2021).
26. R. Su, L.-H. Fan, C. Cao, L. Wang, Z. Du, Z. Cai, Y.-C. Ouyang, Y. Wang, Q. Zhou, L. Wu, N. Zhang, X. Zhu, W.-L. Lei, H. Zhao, Y. Tian, S. He, C. C. L. Wong, Q.-Y. Sun, Y. Xue, Global profiling of RNA-binding protein target sites by LACE-seq. *Nat. Cell Biol.* **23**, 664–675 (2021).
27. Z. Xiong, K. Xu, Z. Lin, F. Kong, Q. Wang, Y. Quan, Q.-q. Sha, F. Li, Z. Zou, L. Liu, S. Ji, Y. Chen, H. Zhang, J. Fang, G. Yu, B. Liu, L. Wang, H. Wang, H. Deng, X. Yang, H.-Y. Fan, L. Li, W. Xie, Ultrasensitive Ribo-seq reveals translational landscapes during mammalian oocyte-to-embryo transition and preimplantation development. *Nat. Cell Biol.* **24**, 968–980 (2022).
28. H. Sun, G. Sun, H. Zhang, H. An, Y. Guo, J. Ge, L. Han, S. Zhu, S. Tang, C. Li, C. Xu, X. Guo, Q. Wang, Proteomic profiling reveals the molecular control of oocyte maturation. *Mol. Cell. Proteomics* **22**, 100481 (2023).
29. J. Hao, Y. Xianfeng, W. Gao, J. Wei, M. Qi, L. Han, S. Shi, C. Lin, D. Wang, The perturbed expression of m6A in parthenogenetic mouse embryos. *Genet. Mol. Biol.* **42**, 666–670 (2019).
30. M. J. Holmes, L. R. Padgett, M. S. Bastos, W. J. Sullivan Jr., m6A RNA methylation facilitates pre-mRNA 3′-end formation and is essential for viability of *Toxoplasma gondii*. *PLOS Pathog.* **17**, e1009335 (2021).
31. M. Anders, I. Chelysheva, I. Goebel, T. Trenkner, J. Zhou, Y. Mao, S. Verzini, S.-B. Qian, Z. Ignatova, Dynamic m^6A methylation facilitates mRNA triaging to stress granules. *Life Sci. Alliance* **1**, e201800113 (2018).
32. H. Chen, H. Yang, X. Zhu, T. Yadav, J. Ouyang, S. S. Truesdell, J. Tan, Y. Wang, M. Duan, L. Wei, L. Zou, A. S. Levine, S. Vasudevan, L. Lan, m^5C modification of mRNA serves a DNA damage code to promote homologous recombination. *Nat. Commun.* **11**, 2834 (2020).
33. A. Svobodová Kovaříková, L. Stixová, A. Kovařík, E. Bártová, PARP-dependent and NAT10-independent acetylation of N4-cytidine in RNA appears in UV-damaged chromatin. *Epigenetics Chromatin* **16**, 26 (2023).
34. S. Sharma, J.-L. Langhendries, P. Watzinger, P. Kötter, K.-D. Entian, D. L. J. Lafontaine, Yeast Kre33 and human NAT10 are conserved 18S rRNA cytosine acetyltransferases that modify tRNAs assisted by the adaptor Tan1/THUMPD1. *Nucleic Acids Res.* **43**, 2242–2258 (2015).
35. S. Ito, S. Horikawa, T. Suzuki, H. Kawauchi, Y. Tanaka, T. Suzuki, T. Suzuki, Human NAT10 is an ATP-dependent RNA acetyltransferase responsible for N4-acetylcytidine formation in 18 S ribosomal RNA (rRNA). *J. Biol. Chem.* **289**, 35724–35730 (2014).
36. S. Ito, Y. Akamatsu, A. Noma, S. Kimura, K. Miyauchi, Y. Ikeuchi, T. Suzuki, T. Suzuki, A single acetylation of 18 S rRNA is essential for biogenesis of the small ribosomal subunit in Saccharomyces cerevisiae. *J. Biol. Chem.* **289**, 26201–26212 (2014).
37. Z. Hu, Y. Lu, J. Cao, L. Lin, X. Chen, Z. Zhou, J. Pu, G. Chen, X. Ma, Q. Deng, Y. Jin, L. Jiang, Y. Li, T. Li, J. Liu, S. Zhu, N-acetyltransferase NAT10 controls cell fates via connecting mRNA cytidine acetylation to chromatin signaling. *Sci. Adv.* **10**, eadh9871 (2024).
38. X. Jiang, Y. Cheng, Y. Zhu, C. Xu, Q. Li, X. Xing, W. Li, J. Zou, L. Meng, M. Azhar, Y. Cao, X. Tong, W. Qin, X. Zhu, J. Bao, Maternal NAT10 orchestrates oocyte meiotic cell-cycle progression and maturation in mice. *Nat. Commun.* **14**, 3729 (2023).
39. G. Balmus, D. Larrieu, A. C. Barros, C. Collins, M. Abrudan, M. Demir, N. J. Geisler, C. J. Lelliott, J. K. White, N. A. Karp, J. Atkinson, A. Kirton, M. Jacobsen, D. Clift, R. Rodriguez, Sanger Mouse Genetics, D. J. Adams, S. P. Jackson, Targeting of NAT10 enhances healthspan in a mouse model of human accelerated aging syndrome. *Nat. Commun.* **9**, 1700 (2018).
40. W. Zhao, Y. Zhou, Q. Cui, Y. Zhou, PACES: Prediction of N4-acetylcytidine (ac4C) modification sites in mRNA. *Sci. Rep.* **9**, 11112 (2019).
41. J. Georgeson, S. Schwartz, No evidence for ac4C within human mRNA upon data reassessment. *Mol. Cell* **84**, 1601–1610.e2 (2024).
42. H. Beiki, D. Sturgill, D. Arango, S. Relier, S. Schiffers, S. Oberdoerffer, Detection of ac4C in human mRNA is preserved upon data reassessment. *Mol. Cell* **84**, 1611–1625.e3 (2024).
43. D. Larrieu, S. Britton, M. Demir, R. Rodriguez, S. P. Jackson, Chemical inhibition of NAT10 corrects defects of laminopathic cells. *Science* **344**, 527–532 (2014).
44. M. J. Johansson, A. S. Bystrom, The Saccharomyces cerevisiae TAN1 gene is required for N4-acetylcytidine formation in tRNA. *RNA* **10**, 712–719 (2004).
45. Q. Q. Sha, J. Zhang, H. Y. Fan, A story of birth and death: mRNA translation and clearance at the onset of maternal-to-zygotic transition in mammalsdagger. *Biol. Reprod.* **101**, 579–590 (2019).
46. Z. Y. Jiang, H. Y. Fan, Five questions toward mRNA degradation in oocytes and preimplantation embryos: when, who, to whom, how, and why?dagger. *Biol. Reprod.* **107**, 62–75 (2022).
47. G. Jin, M. Xu, M. Zou, S. Duan, The processing, gene regulation, biological functions, and clinical relevance of N4-acetylcytidine on RNA: A systematic review. *Mol. Ther. Nucleic Acids* **20**, 13–24 (2020).
48. Z. J. Lan, X. Xu, A. J. Cooney, Differential oocyte-specific expression of Cre recombinase activity in GDF-9-iCre, Zp3cre, and Msx2Cre transgenic mice. *Biol. Reprod.* **71**, 1469–1474 (2004).
49. B. Langmead, S. L. Salzberg, Fast gapped-read alignment with Bowtie 2. *Nat. Methods* **9**, 357–359 (2012).
50. D. Kim, J. M. Paggi, C. Park, C. Bennett, S. L. Salzberg, Graph-based genome alignment and genotyping with HISAT2 and HISAT-genotype. *Nat. Biotechnol.* **37**, 907–915 (2019).
51. A. Tarasov, A. J. Vilella, E. Cuppen, I. J. Nijman, P. Prins, Sambamba: Fast processing of NGS alignment formats. *Bioinformatics* **31**, 2032–2034 (2015).

52. F. Ramirez, F. Dundar, S. Diehl, B. A. Gruning, T. Manke, deepTools: A flexible platform for exploring deep-sequencing data. *Nucleic Acids Res.* **42**, W187–W191 (2014).
53. Y. Zhang, T. Liu, C. A. Meyer, J. Eeckhoute, D. S. Johnson, B. E. Bernstein, C. Nusbaum, R. M. Myers, M. Brown, W. Li, X. S. Liu, Model-based analysis of ChIP-Seq (MACS). *Genome Biol.* **9**, R137 (2008).
54. A. R. Quinlan, I. M. Hall, BEDTools: A flexible suite of utilities for comparing genomic features. *Bioinformatics* **26**, 841–842 (2010).

Acknowledgments: We thank all members of the laboratory for fruitful discussions and valuable suggestions. We also thank the Core Facility of Life Sciences Institute, Zhejiang University for assistance with the experiments. **Funding:** This work was supported by the following: National Key Research and Development Program of China (2021YFC2700100) to H.-Y.F., National Natural Science Foundation of China (31930031 and 32072939) to H.-Y.F., Key Research and Development Program of Zhejiang Province (2021C03100 and 2021C03098) to H.-Y.F., Natural Science Foundation of Zhejiang Province (LD22C060001) to H.-Y.F., fellowship of China National Postdoctoral Program for Innovative Talents (BX20230031) to L.C., National Natural Science Foundation of China (32400703) to L.C., Beijing Natural Science Foundation (7244435) to L.C., and fellowship of China Postdoctoral Science Foundation (2023M740143) to L.C. **Author contributions:** Conceptualization: L.C., S.-Y.L., Q.-Q.S., and H.-Y.F. Data curation: Y.-K.W., S.-Y.L., and H.-Y.F. Formal analysis: L.C., Y.-K.W., S.-Y.L., R.-B.S., Q.-Q.S., and H.-Y.F. Funding acquisition: L.C., Q.-Q.S., and H.-Y.F. Investigation: L.C., W.-J.W., S.-Y.L., Q.-Q.S., and H.-Y.F. Methodology: L.C., W.-J.W., R.-B.S., Q.-Q.S., and H.-Y.F. Project administration: L.C. and H.-Y.F Software: S.-Y.L., Y.-K.W., Q.-Q.S., and H.-Y.F Resources: Y.-K.W. and H.-Y.F. Validation: L.C., W.-J.W., S.-Y.L., R.-B.S., Q.-Q.S., and H.-Y.F. Visualization: L.C., W.-J.W., S.-Y.L., R.-B.S., Y.-K.W., X.W., Q.-Q.S., and H.-Y.F. Supervision: H.-Y.F. Writing—original draft: L.C., S.-Y.L., and H.-Y.F. Writing—review and editing: L.C., S.-Y.L., R.-B.S., S.-Y.Z., J.Q., Q.-Q.S., and H.-Y.F. **Competing interests:** The authors declare that they have no competing interests. **Data and materials availability:** RNA-seq and ac^4C LACE-seq raw data have been deposited in the NCBI Gene Expression Omnibus database (https://www.ncbi.nlm.nih.gov). The RNA-seq raw data are under accession code GSE254288. The ac^4C and NAT10 LACE-seq data created in this study are available from the GEO database, and the accession number is GSE253976. All data needed to evaluate the conclusions in the paper are present in the paper and/or the Supplementary Materials.

Submitted 28 March 2024
Accepted 17 January 2025
Published 21 February 2025
10.1126/sciadv.adp5163